The Astrophysical Journal Supplement Series, 219:12 (27pp), 2015 July doi:10.1088/0067-0049/219/1/12

THE ELEVENTH AND TWELFTH DATA RELEASES OF THE SLOAN DIGITAL SKY SURVEY: FINAL DATA FROM SDSS-III

Shadab Alam[1], Franco D. Albareti[2], Carlos Allende Prieto[3,4], F. Anders[5], Scott F. Anderson[6], Timothy Anderton[7], Brett H. Andrews[8,9], Eric Armengaud[10], Éric Aubourg[11], Stephen Bailey[12], Sarbani Basu[13], Julian E. Bautista[11], Rachael L. Beaton[14,15], Timothy C. Beers[16], Chad F. Bender[17,18], Andreas A. Berlind[19], Florian Beutler[12], Vaishali Bhardwaj[6,12], Jonathan C. Bird[19], Dmitry Bizyaev[20,21,22], Cullen H. Blake[23], Michael R. Blanton[24], Michael Blomqvist[25], John J. Bochanski[6,26], Adam S. Bolton[7], Jo Bovy[27,136], A. Shelden Bradley[20], W. N. Brandt[17,28,29], D. E. Brauer[5], J. Brinkmann[20], Peter J. Brown[30], Joel R. Brownstein[7], Angela Burden[31], Etienne Burtin[10], Nicolás G. Busca[11,32,33], Zheng Cai[34], Diego Capozzi[31], Aurelio Carnero Rosell[32,33], Michael A. Carr[35], Ricardo Carrera[3,4], K. C. Chambers[36], William James Chaplin[37,38], Yen-Chi Chen[39], Cristina Chiappini[5,33], S. Drew Chojnowski[21], Chia-Hsun Chuang[2], Nicolas Clerc[40], Johan Comparat[2], Kevin Covey[41,42], Rupert A. C. Croft[1], Antonio J. Cuesta[43,44], Katia Cunha[32,34], Luiz N. da Costa[32,33], Nicola Da Rio[45], James R. A. Davenport[6], Kyle S. Dawson[7], Nathan De Lee[46], Timothée Delubac[47], Rohit Deshpande[17,18], Saurav Dhital[48], Letícia Dutra-Ferreira[33,49,50], Tom Dwelly[40], Anne Ealet[51], Garrett L. Ebelke[14], Edward M. Edmondson[31], Daniel J. Eisenstein[52], Tristan Ellsworth[7], Yvonne Elsworth[37,38], Courtney R. Epstein[8], Michael Eracleous[6,17,28,53], Stephanie Escoffier[51], Massimiliano Esposito[3,4], Michael L. Evans[6], Xiaohui Fan[34], Emma Fernández-Alvar[3,4], Diane Feuillet[21], Nurten Filiz Ak[17,28,54], Hayley Finley[55], Alexis Finoguenov[56], Kevin Flaherty[57], Scott W. Fleming[58,59], Andreu Font-Ribera[12], Jonathan Foster[44], Peter M. Frinchaboy[60], J. G. Galbraith-Frew[7], Rafael A. García[61], D. A. García-Hernández[3,4], Ana E. García Pérez[3,4,14], Patrick Gaulme[20], Jian Ge[45], R. Génova-Santos[3,4], A. Georgakakis[40], Luan Ghezzi[32,52], Bruce A. Gillespie[62], Léo Girardi[33,63], Daniel Goddard[31], Satya Gontcho A Gontcho[43], Jonay I. González Hernández[3,4], Eva K. Grebel[64], Paul J. Green[52], Jan Niklas Grieb[40], Nolan Grieves[45], James E. Gunn[35], Hong Guo[7], Paul Harding[65], Sten Hasselquist[21], Suzanne L. Hawley[6], Michael Hayden[21], Fred R. Hearty[17], Saskia Hekker[38,66], Shirley Ho[1], David W. Hogg[24], Kelly Holley-Bockelmann[19], Jon A. Holtzman[21], Klaus Honscheid[67,68], Daniel Huber[38,69,70], Joseph Huehnerhoff[20], Inese I. Ivans[7], Linhua Jiang[71], Jennifer A. Johnson[8,68], Karen Kinemuchi[20,21], David Kirkby[25], Francisco Kitaura[5], Mark A. Klaene[20], Gillian R. Knapp[35], Jean-Paul Kneib[47,72], Xavier P. Koenig[13], Charles R. Lam[14], Ting-Wen Lan[62], Dustin Lang[1], Pierre Laurent[10], Jean-Marc Le Goff[10], Alexie Leauthaud[73], Khee-Gan Lee[74], Young Sun Lee[75], Timothy C. Licquia[9], Jian Liu[45], Daniel C. Long[20,21], Martín López-Corredoira[3,4], Diego Lorenzo-Oliveira[33,49], Sara Lucatello[63], Britt Lundgren[76], Robert H. Lupton[35], Claude E. Mack III[5,19], Suvrath Mahadevan[17,18], Marcio A. G. Maia[32,33], Steven R. Majewski[14], Elena Malanushenko[20,21], Viktor Malanushenko[20,21], A. Manchado[3,4], Marc Manera[31,77], Qingqing Mao[19], Claudia Maraston[31], Robert C. Marchwinski[17,18], Daniel Margala[25], Sarah L. Martell[78], Marie Martig[74], Karen L. Masters[31], Savita Mathur[79], Cameron K. McBride[52], Peregrine M. McGehee[80], Ian D. McGreer[34], Richard G. McMahon[81,82], Brice Ménard[62,73,137], Marie-Luise Menzel[40], Andrea Merloni[40], Szabolcs Mészáros[83], Adam A. Miller[84,85,138], Jordi Miralda-Escudé[43,86], Hironao Miyatake[35,73], Antonio D. Montero-Dorta[7], Surhud More[73], Eric Morganson[52], Xan Morice-Atkinson[31], Heather L. Morrison[65], Benoît Mosser[87], Demitri Muna[8], Adam D. Myers[88], Kirpal Nandra[40], Jeffrey A. Newman[9], Mark Neyrinck[62], Duy Cuong Nguyen[89], Robert C. Nichol[31], David L. Nidever[90], Pasquier Noterdaeme[55], Sebastián E. Nuza[5], Julia E. O'Connell[60], Robert W. O'Connell[14], Ross O'Connell[1], Ricardo L. C. Ogando[32,33], Matthew D. Olmstead[7,91], Audrey E. Oravetz[20,21], Daniel J. Oravetz[20], Keisuke Osumi[1], Russell Owen[6], Deborah L. Padgett[92], Nikhil Padmanabhan[44], Martin Paegert[19], Nathalie Palanque-Delabrouille[10], Kaike Pan[20], John K. Parejko[93], Isabelle Pâris[94], Changbom Park[95], Petchara Pattarakijwanich[35], M. Pellejero-Ibanez[3,4], Joshua Pepper[19,96], Will J. Percival[31], Ismael Pérez-Fournon[3,4], Ignasi Peŕez-Rafols[43,97], Patrick Petitjean[55], Matthew M. Pieri[31,98], Marc H. Pinsonneault[8], Gustavo F. Porto de Mello[33,49], Francisco Prada[2,99,100], Abhishek Prakash[9], Adrian M. Price-Whelan[101], Pavlos Protopapas[102], M. Jordan Raddick[62], Mubdi Rahman[62], Beth A. Reid[12,103], James Rich[10], Hans-Walter Rix[74], Annie C. Robin[104], Constance M. Rockosi[105], Thaíse S. Rodrigues[33,63,106], Sergio Rodríguez-Torres[2,99], Natalie A. Roe[12], Ashley J. Ross[31,68], Nicholas P. Ross[107], Graziano Rossi[10,108], John J. Ruan[6], J. A. Rubiño-Martín[3,4], Eli S. Rykoff[109], Salvador Salazar-Albornoz[40,110], Mara Salvato[40,111], Lado Samushia[112,113], Ariel G. Sánchez[40], Basílio Santiago[33,114], Conor Sayres[6], Ricardo P. Schiavon[115,116], David J. Schlegel[12], Sarah J. Schmidt[8], Donald P. Schneider[17,28], Mathias Schultheis[117], Axel D. Schwope[5], C. G. Scóccola[3,4], Caroline Scott[52], Kris Sellgren[8], Hee-Jong Seo[118], Aldo Serenelli[119], Neville Shane[14], Yue Shen[15,71], Matthew Shetrone[120], Yiping Shu[7], V. Silva Aguirre[38], Thirupathi Sivarani[121], M. F. Skrutskie[14], Anže Slosar[122], Verne V. Smith[123], Flávia Sobreira[33,124], Diogo Souto[32], Keivan G. Stassun[19,125], Matthias Steinmetz[5], Dennis Stello[38,69], Michael A. Strauss[35,139], Alina Streblyanska[3,4], Nao Suzuki[73], Molly E. C. Swanson[52], Jonathan C. Tan[45], Jamie Tayar[8], Ryan C. Terrien[17,18,126], Aniruddha R. Thakar[62], Daniel Thomas[31,127], Neil Thomas[45], Benjamin A. Thompson[60], Jeremy L. Tinker[24], Rita Tojeiro[128], Nicholas W. Troup[14], Mariana Vargas-Magaña[1],

Jose A. Vazquez[122], Licia Verde[43,86,129], Matteo Viel[94,130], Nicole P. Vogt[21], David A. Wake[76,131], Ji Wang[13], Benjamin A. Weaver[24], David H. Weinberg[8], Benjamin J. Weiner[34], Martin White[12,103], John C. Wilson[14], John P. Wisniewski[132], W. M. Wood-Vasey[9,139], Christophe Yèche[10], Donald G. York[133], Nadia L. Zakamska[62], O. Zamora[3,4], Gail Zasowski[62], Idit Zehavi[65], Gong-Bo Zhao[31,134], Zheng Zheng[7], Xu Zhou (周旭)[135], Zhimin Zhou (周志民)[135], Hu Zou (邹虎)[135], and Guangtun Zhu[62,138]

[1] McWilliams Center for Cosmology, Department of Physics, Carnegie Mellon University, 5000 Forbes Ave, Pittsburgh, PA 15213, USA
[2] Instituto de Física Teórica, (UAM/CSIC), Universidad Autónoma de Madrid, Cantoblanco, E-28049 Madrid, Spain
[3] Instituto de Astrofísica de Canarias (IAC), C/Vía Láctea, s/n, E-38200, La Laguna, Tenerife, Spain
[4] Departamento de Astrofísica, Universidad de La Laguna, E-38206, La Laguna, Tenerife, Spain
[5] Leibniz-Institut für Astrophysik Potsdam (AIP), An der Sternwarte 16, D-14482 Potsdam, Germany
[6] Department of Astronomy, University of Washington, Box 351580, Seattle, WA 98195, USA
[7] Department of Physics and Astronomy, University of Utah, Salt Lake City, UT 84112, USA
[8] Department of Astronomy, Ohio State University, 140 West 18th Avenue, Columbus, OH 43210, USA
[9] PITT PACC, Department of Physics and Astronomy, University of Pittsburgh, 3941 O'Hara Street, Pittsburgh, PA 15260, USA
[10] CEA, Centre de Saclay, Irfu/SPP, F-91191 Gif-sur-Yvette, France
[11] APC, University of Paris Diderot, CNRS/IN2P3, CEA/IRFU, Observatoire de Paris, Sorbonne Paris Cité, F-75205 Paris, France
[12] Lawrence Berkeley National Laboratory, One Cyclotron Road, Berkeley, CA 94720, USA
[13] Department of Astronomy, Yale University, P.O. Box 208101, New Haven, CT 06520-8101, USA
[14] Department of Astronomy, University of Virginia, P.O. Box 400325, Charlottesville, VA 22904-4325, USA
[15] Observatories of the Carnegie Institution of Washington, 813 Santa Barbara Street, Pasadena, CA 91101, USA
[16] Department of Physics and JINA Center for the Evolution of the Elements, University of Notre Dame, Notre Dame, IN 46556, USA
[17] Department of Astronomy and Astrophysics, 525 Davey Laboratory, The Pennsylvania State University, University Park, PA 16802, USA
[18] Center for Exoplanets and Habitable Worlds, 525 Davey Laboratory, Pennsylvania State University, University Park, PA 16802, USA
[19] Department of Physics and Astronomy, Vanderbilt University, VU Station 1807, Nashville, TN 37235, USA
[20] Apache Point Observatory, P.O. Box 59, Sunspot, NM 88349, USA
[21] Department of Astronomy, MSC 4500, New Mexico State University, P.O. Box 30001, Las Cruces, NM 88003, USA
[22] Sternberg Astronomical Institute, Moscow State University, Universitetskij Prosp. 13, Moscow 119992, Russia
[23] University of Pennsylvania, Department of Physics and Astronomy, 219 South 33rd Street, Philadelphia, PA 19104, USA
[24] Center for Cosmology and Particle Physics, Department of Physics, New York University, 4 Washington Place, New York, NY 10003, USA
[25] Department of Physics and Astronomy, University of California, Irvine, CA 92697, USA
[26] Rider University, 2083 Lawrenceville Road, Lawrenceville, NJ 08648, USA
[27] Institute for Advanced Study, Einstein Drive, Princeton, NJ 08540, USA
[28] Institute for Gravitation and the Cosmos, The Pennsylvania State University, University Park, PA 16802, USA
[29] Department of Physics, The Pennsylvania State University, University Park, PA 16802, USA
[30] George P. and Cynthia Woods Mitchell Institute for Fundamental Physics and Astronomy, Texas A. and M. University, Department of Physics and Astronomy, 4242 TAMU, College Station, TX 77843, USA
[31] Institute of Cosmology and Gravitation, Dennis Sciama Building, University of Portsmouth, Portsmouth, PO1 3FX, UK
[32] Observatório Nacional, Rua Gal. José Cristino 77, Rio de Janeiro, RJ—20921-400, Brazil
[33] Laboratório Interinstitucional de e-Astronomia, - LIneA, Rua Gal.José Cristino 77, Rio de Janeiro, RJ—20921-400, Brazil
[34] Steward Observatory, 933 North Cherry Avenue, Tucson, AZ 85721, USA
[35] Department of Astrophysical Sciences, Princeton University, Princeton, NJ 08544, USA
[36] Institute for Astronomy, University of Hawaii, 2680 Woodlawn Drive, Honolulu, HI 96822, USA
[37] School of Physics and Astronomy, University of Birmingham, Birmingham B15 2TT, UK
[38] Stellar Astrophysics Centre (SAC), Department of Physics and Astronomy, Aarhus University, Ny Munkegade 120, DK-8000 Aarhus C, Denmark
[39] Department of Statistics, Bruce and Astrid McWilliams Center for Cosmology, Carnegie Mellon University, 5000 Forbes Avenue, Pittsburgh, PA 15213, USA
[40] Max-Planck-Institut für Extraterrestrische Physik, Postfach 1312, Giessenbachstrasse D-85741 Garching, Germany
[41] Lowell Observatory, 1400 W. Mars Hill Road, Flagstaff AZ 86001, USA
[42] Western Washington University, Department of Physics & Astronomy, 516 High Street, Bellingham WA 98225, USA
[43] Institut de Ciències del Cosmos, Universitat de Barcelona/IEEC, Barcelona E-08028, Spain
[44] Yale Center for Astronomy and Astrophysics, Yale University, New Haven, CT, 06520, USA
[45] Department of Astronomy, University of Florida, Bryant Space Science Center, Gainesville, FL 32611-2055, USA
[46] Department of Physics and Geology, Northern Kentucky University, Highland Heights, KY 41099, USA
[47] Laboratoire d'Astrophysique, École Polytechnique Fédérale de Lausanne (EPFL), Observatoire de Sauverny, 1290, Versoix, Switzerland
[48] Department of Physical Sciences, Embry-Riddle Aeronautical University, 600 South Clyde Morris Boulevard, Daytona Beach, FL 32114, USA
[49] Universidade Federal do Rio de Janeiro, Observatório do Valongo, Ladeira do Pedro Antônio 43, 20080-090 Rio de Janeiro, Brazil
[50] Departamento de Física, Universidade Federal do Rio Grande do Norte, 59072-970, Natal, RN, Brazil
[51] Centre de Physique des Particules de Marseille, Aix-Marseille Université, CNRS/IN2P3, F-13288 Marseille, France
[52] Harvard-Smithsonian Center for Astrophysics, 60 Garden Street, Cambridge MA 02138, USA
[53] Center for Relativistic Astrophysics, Georgia Institute of Technology, Atlanta, GA 30332, USA
[54] Faculty of Sciences, Department of Astronomy and Space Sciences, Erciyes University, 38039 Kayseri, Turkey
[55] Institut d'Astrophysique de Paris, UPMC-CNRS, UMR7095, 98 bis Boulevard Arago, F-75014, Paris, France
[56] Department of Physics, University of Helsinki, Gustaf Hällströmin katu 2, Helsinki FI-00140, Finland
[57] Department of Astronomy, Van Vleck Observatory, Wesleyan University, Middletown, CT 06459, USA
[58] Space Telescope Science Institute, 3700 San Martin Drive, Baltimore, MD 21218, USA
[59] Computer Sciences Corporation, 3700 San Martin Drive, Baltimore, MD 21218, USA
[60] Department of Physics and Astronomy, Texas Christian University, 2800 South University Drive, Fort Worth, TX 76129, USA
[61] Laboratoire AIM, CEA/DSM—CNRS—Univ. Paris Diderot—IRFU/SAp, Centre de Saclay, F-91191 Gif-sur-Yvette Cedex, France
[62] Center for Astrophysical Sciences, Department of Physics and Astronomy, Johns Hopkins University, 3400 North Charles Street, Baltimore, MD 21218, USA
[63] INAF, Osservatorio Astronomico di Padova, Vicolo dell'Osservatorio 5, I-35122 Padova, Italy
[64] Astronomisches Rechen-Institut, Zentrum für Astronomie der Universität Heidelberg, Mönchhofstrasse 12-14, D-69120 Heidelberg, Germany
[65] Department of Astronomy, Case Western Reserve University, Cleveland, OH 44106, USA
[66] Max-Planck-Institut für Sonnensystemforschung, Justus-von-Liebig-Weg 3, D-37077 Göttingen, Germany
[67] Department of Physics, Ohio State University, Columbus, OH 43210, USA
[68] Center for Cosmology and Astro-Particle Physics, Ohio State University, Columbus, OH 43210, USA
[69] Sydney Institute for Astronomy (SIfA), School of Physics, University of Sydney, Sydney, NSW 2006, Australia

[70] SETI Institute, 189 Bernardo Avenue, Mountain View, CA 94043, USA
[71] Kavli Institute for Astronomy and Astrophysics, Peking University, Beijing 100871, China
[72] Laboratoire d'Astrophysique de Marseille, CNRS-Université de Provence, 38 rue F. Joliot-Curie, F-13388 Marseille cedex 13, France
[73] Kavli Institute for the Physics and Mathematics of the Universe (Kavli IPMU, WPI), Todai Institutes for Advanced Study, The University of Tokyo, Kashiwa, 277-8583, Japan
[74] Max-Planck-Institut für Astronomie, Königstuhl 17, D-69117 Heidelberg, Germany
[75] Department of Astronomy and Space Science Chungnam National University Daejeon 305-764, Korea
[76] Department of Astronomy, University of Wisconsin-Madison, 475 North Charter Street, Madison WI 53703, USA
[77] University College London, Gower Street, London, WC1E 6BT, UK
[78] School of Physics, University of New South Wales, Sydney, NSW 2052, Australia
[79] Space Science Institute, 4750 Walnut Street, Suite 205, Boulder, CO 80301, USA
[80] IPAC, MS 220-6, California Institute of Technology, Pasadena, CA 91125, USA
[81] Institute of Astronomy, University of Cambridge, Madingley Road, Cambridge CB3 0HA, UK
[82] Kavli Institute for Cosmology, University of Cambridge, Madingley Road, Cambridge CB3 0HA, UK
[83] ELTE Gothard Astrophysical Observatory, H-9704 Szombathely, Szent Imre herceg st. 112, Hungary
[84] Jet Propulsion Laboratory, California Institute of Technology, Pasadena, CA 91109, USA
[85] Department of Astronomy, California Institute of Technology, Pasadena, CA 91125, USA
[86] Institució Catalana de Recerca i Estudis Avançats, Barcelona E-08010, Spain
[87] LESIA, UMR 8109, Université Pierre et Marie Curie, Université Denis Diderot, Observatoire de Paris, F-92195 Meudon Cedex, France
[88] Department of Physics and Astronomy, University of Wyoming, Laramie, WY 82071, USA
[89] Dunlap Institute for Astronomy and Astrophysics, University of Toronto, Toronto, ON, M5S 3H4, Canada
[90] Dept. of Astronomy, University of Michigan, Ann Arbor, MI, 48104, USA
[91] Department of Chemistry and Physics, King's College, Wilkes-Barre, PA 18711, USA
[92] NASA/GSFC, Code 665, Greenbelt, MC 20770, USA
[93] Department of Physics, Yale University, 260 Whitney Avenue, New Haven, CT, 06520, USA
[94] INAF, Osservatorio Astronomico di Trieste, Via G. B. Tiepolo 11, I-34131 Trieste, Italy
[95] School of Physics, Korea Institute for Advanced Study, 85 Hoegiro, Dongdaemun-gu, Seoul 130-722, Korea
[96] Department of Physics, Lehigh University, 16 Memorial Drive East, Bethlehem, PA 18015, USA
[97] Departament d'Astronomia i Meteorologia, Facultat de Física, Universitat de Barcelona, E-08028 Barcelona, Spain
[98] A*MIDEX, Aix Marseille Université, CNRS, LAM (Laboratoire d'Astrophysique de Marseille) UMR 7326, F-13388 Marseille cedex 13, France
[99] Campus of International Excellence UAM+CSIC, Cantoblanco, E-28049 Madrid, Spain
[100] Instituto de Astrofísica de Andalucía (CSIC), Glorieta de la Astronomía, E-18080 Granada, Spain
[101] Department of Astronomy, Columbia University, New York, NY 10027, USA
[102] Institute for Applied Computational Science, SEAS, Harvard University, 52 Oxford Street, Cambridge, MA 02138, USA
[103] Department of Physics, University of California, Berkeley, CA 94720, USA
[104] Université de Franche-Comté, Institut Utinam, UMR CNRS 6213, OSU Theta, Besançon, F-25010, France
[105] Department of Astronomy and Astrophysics, University of California, Santa Cruz, 1156 High Street, Santa Cruz, CA 95064, USA
[106] Dipartimento di Fisica e Astronomia, Università di Padova, Vicolo dell'Osservatorio 2, I-35122 Padova, Italy
[107] Department of Physics, Drexel University, 3141 Chestnut Street, Philadelphia, PA 19104, USA
[108] Department of Astronomy and Space Science, Sejong University, Seoul, 143-747, Korea
[109] SLAC National Accelerator Laboratory, Menlo Park, CA 94025, USA
[110] Universitäts-Sternwarte München, Scheinerstrasse 1, D-81679 Munich, Germany
[111] Cluster of Excellence, Boltzmannstraße 2, D-85748 Garching, Germany
[112] Department of Physics, Kansas State University, 116 Cardwell Hall, Manhattan, KS 66506, USA
[113] National Abastumani Astrophysical Observatory, Ilia State University, 2A Kazbegi Ave., GE-1060 Tbilisi, Georgia
[114] Instituto de Física, UFRGS, Caixa Postal 15051, Porto Alegre, RS—91501-970, Brazil
[115] Gemini Observatory, 670 N. A'Ohoku Place, Hilo, HI 96720, USA
[116] Astrophysics Research Institute, Liverpool John Moores University, IC2, Liverpool Science Park, 146 Brownlow Hill, Liverpool L3 5RF, UK
[117] Université de Nice Sophia-Antipolis, CNRS, Observatoire de Côte d'Azur, Laboratoire Lagrange, BP 4229, F-06304 Nice Cedex 4, France
[118] Department of Physics and Astronomy, Ohio University, 251B Clippinger Labs, Athens, OH 45701, USA
[119] Instituto de Ciencias del Espacio (CSIC-IEEC), Facultad de Ciencias, Campus UAB, E-08193, Bellaterra, Spain
[120] University of Texas at Austin, Hobby-Eberly Telescope, 32 Fowlkes Road, McDonald Observatory, TX 79734-3005, USA
[121] Indian Institute of Astrophysics, II Block, Koramangala, Bangalore 560 034, India
[122] Brookhaven National Laboratory, Bldg 510, Upton, NY 11973, USA
[123] National Optical Astronomy Observatory, 950 North Cherry Avenue, Tucson, AZ, 85719, USA
[124] Fermi National Accelerator Laboratory, P.O. Box 500, Batavia, IL 60510, USA
[125] Department of Physics, Fisk University, 1000 17th Avenue North, Nashville, TN 37208, USA
[126] The Penn State Astrobiology Research Center, Pennsylvania State University, University Park, PA 16802, USA
[127] SEPnet, South East Physics Network, UK
[128] School of Physics and Astronomy, University of St Andrews, St Andrews, Fife, KY16 9SS, UK
[129] Institute of Theoretical Astrophysics, University of Oslo, NO-0315 Oslo, Norway
[130] INFN/National Institute for Nuclear Physics, Via Valerio 2, I-34127 Trieste, Italy
[131] Department of Physical Sciences, The Open University, Milton Keynes MK7 6AA, UK
[132] H.L. Dodge Department of Physics and Astronomy, University of Oklahoma, Norman, OK 73019, USA
[133] Department of Astronomy and Astrophysics and the Enrico Fermi Institute, University of Chicago, 5640 South Ellis Avenue, Chicago, IL 60637, USA
[134] National Astronomical Observatories, Chinese Academy of Sciences, Beijing, 100012, China
[135] Key Laboratory of Optical Astronomy, National Astronomical Observatories, Chinese Academy of Sciences, Beijing, 100012, China
Received 2015 January 7; accepted 2015 April 2; published 2015 July 27

[136] John Bahcall Fellow.
[137] Alfred P. Sloan Fellow.
[138] Hubble Fellow.
[139] Corresponding authors.

ABSTRACT

The third generation of the Sloan Digital Sky Survey (SDSS-III) took data from 2008 to 2014 using the original SDSS wide-field imager, the original and an upgraded multi-object fiber-fed optical spectrograph, a new near-infrared high-resolution spectrograph, and a novel optical interferometer. All of the data from SDSS-III are now made public. In particular, this paper describes Data Release 11 (DR11) including all data acquired through 2013 July, and Data Release 12 (DR12) adding data acquired through 2014 July (including all data included in previous data releases), marking the end of SDSS-III observing. Relative to our previous public release (DR10), DR12 adds one million new spectra of galaxies and quasars from the Baryon Oscillation Spectroscopic Survey (BOSS) over an additional 3000 deg^2 of sky, more than triples the number of H-band spectra of stars as part of the Apache Point Observatory (APO) Galactic Evolution Experiment (APOGEE), and includes repeated accurate radial velocity measurements of 5500 stars from the Multi-object APO Radial Velocity Exoplanet Large-area Survey (MARVELS). The APOGEE outputs now include the measured abundances of 15 different elements for each star. In total, SDSS-III added 5200 deg^2 of ugriz imaging; 155,520 spectra of 138,099 stars as part of the Sloan Exploration of Galactic Understanding and Evolution 2 (SEGUE-2) survey; 2,497,484 BOSS spectra of 1,372,737 galaxies, 294,512 quasars, and 247,216 stars over 9376 deg^2; 618,080 APOGEE spectra of 156,593 stars; and 197,040 MARVELS spectra of 5513 stars. Since its first light in 1998, SDSS has imaged over 1/3 of the Celestial sphere in five bands and obtained over five million astronomical spectra.

Key words: atlases – catalogs – surveys

1. INTRODUCTION

Comprehensive wide-field imaging and spectroscopic surveys of the sky have played a key role in astronomy, leading to fundamental new breakthroughs in our understanding of the Solar System; our Milky Way Galaxy and its constituent stars and gas; the nature, properties, and evolution of galaxies; and the universe as a whole. The Sloan Digital Sky Survey (SDSS), which started routine operations in 2000 April, has carried out imaging and spectroscopy over roughly 1/3 of the Celestial Sphere. SDSS uses a dedicated 2.5 m wide-field telescope (Gunn et al. 2006), instrumented with a sequence of sophisticated imagers and spectrographs. The SDSS has gone through a series of stages. SDSS-I (York et al. 2000), which was in operation through 2005, focused on a "Legacy" survey of five-band imaging (using what was at the time the largest camera ever used in optical astronomy; Gunn et al. 1998) and spectroscopy of well-defined samples of galaxies (Eisenstein et al. 2001; Strauss et al. 2002) and quasars (Richards et al. 2002), using a 640 fiber pair of spectrographs (Smee et al. 2013). SDSS-II operated from 2005 to 2008 and finished the Legacy survey. It also carried out a repeated imaging survey of the Celestial Equator in the Fall sky to search for supernovae (Frieman et al. 2008), as well as a spectroscopic survey of stars to study the structure of the Milky Way (Yanny et al. 2009).

SDSS-III (Eisenstein et al. 2011) started operations in Fall 2008, completing in Summer 2014. SDSS-III consisted of four interlocking surveys.

1. The Sloan Exploration of Galactic Understanding and Evolution 2 (SEGUE-2; C. Rockosi et al. 2015, in preparation) used the SDSS-I/II spectrographs to obtain R ~ 2000 spectra of stars at high and low Galactic latitudes to study Galactic structure, dynamics, and stellar populations. SEGUE-2 gathered data during the 2008–2009 season.
2. The Baryon Oscillation Spectroscopic Survey (BOSS; Dawson et al. 2013) used the SDSS imager to increase the footprint of SDSS imaging in the southern Galactic Cap in the 2008–2009 season. The SDSS spectrographs were then completely rebuilt with new fibers (2″ entrance aperture rather than 3″, 1000 fibers per exposure) as well as new gratings, CCDs, and optics. Galaxies (B. Reid et al. 2015, in preparation) and quasars (Ross et al. 2012) were selected from the SDSS imaging data, and are used to study the baryon oscillation feature in the clustering of galaxies (Anderson et al. 2014a, 2014c) and Lyα absorption along the line of sight to distant quasars (Busca et al. 2013; Slosar et al. 2013; Font-Ribera et al. 2014; Delubac et al. 2015). BOSS collected spectroscopic data from 2009 December to 2014 July.
3. The Apache Point Observatory Galaxy Evolution Experiment (APOGEE; S. Majewski et al. 2015, in preparation) used a separate 300 fiber high-resolution (R ~ 22,500), H-band spectrograph to investigate the composition and dynamics of stars in the Galaxy. The target stars were selected from the 2MASS database (Skrutskie et al. 2006); the resulting spectra give highly accurate stellar surface temperatures, gravities, and detailed abundance measurements. APOGEE gathered data from 2011 May to 2014 July.
4. The Multi-object APO Radial Velocity Exoplanet Large-area Survey (MARVELS; J. Ge et al. 2015, in preparation) used a 60 fiber interferometric spectrograph to measure the high-precision radial velocities (RVs) of stars to search for extra-solar planets and brown dwarfs orbiting them. MARVELS gathered data from 2008 October to 2012 July.

The SDSS data have been made available to the scientific community and the public in a roughly annual cumulative series of data releases. These data have been distributed (Thakar 2008b) in the form of direct access to raw and processed imaging and spectral files and also through a relational database (the "Catalog Archive Server," or "CAS"), presenting the derived catalog information. As of DR12, these catalogs present information on a total of ~470 million objects in the imaging survey and 5.3 million spectra.

The Early Data Release (EDR; Stoughton et al. 2002) and Data Releases 1–5 (DR1; Abazajian et al. 2003, DR2; Abazajian et al. 2004, DR3; Abazajian et al. 2005, DR4; Adelman-McCarthy et al. 2006, and DR5; Adelman-McCarthy et al. 2007) included data from SDSS-I. DR6 and DR7 (Adelman-McCarthy et al. 2008; Abazajian et al. 2009)

covered the data in SDSS-II. The data from SDSS-III have appeared in three releases thus far. DR8 (Aihara et al. 2011) included the final data from the SDSS imaging camera, as well as all the SEGUE-2 data. DR9 (Ahn et al. 2012) included the first spectroscopic data from BOSS. DR10 (Ahn et al. 2014) roughly doubled the amount of BOSS data made public and included the first release of APOGEE data.

The SDSS-III collaboration has found it useful to internally define a data set associated with the data taken through 2013 Summer, which we designate as "DR11." The SDSS-III completed data-taking in 2014 July, and the present paper describes both DR11 and Data Release 12 (DR12). Like previous data releases, DR12 is cumulative; it includes all of the data taken by SDSS to date. DR12 includes almost 2.5 million BOSS spectra of quasars, galaxies, and stars over 9376 square degrees: 155,000 SEGUE-2 spectra of 138,000 stars (as released in DR8), and 618,000 APOGEE spectra of 156,000 stars. It also includes the first release of MARVELS data, presenting 197,000 spectra of 5500 stars (3300 stars with >16 observations each). Because some BOSS, APOGEE, and MARVELS scientific papers have been based on the DR11 sample, this paper describes the distinction between DR11 and DR12 and the processing software for the two data sets, and how to understand this distinction in the database.

The data release itself may be accessed from the SDSS-III website[140] or the DR12 page of the new pan-SDSS website.[141] DR11 is similarly available through the same interfaces. The outline of this paper is as follows. We summarize the full contents of DR11 and DR12 in Section 2, emphasizing the quantity of spectra and the solid angle covered by each of the surveys. Details for each component of SDSS-III are described in Section 3 (MARVELS), Section 4 (BOSS), and Section 5 (APOGEE). There have been no updates to SEGUE-2 since DR9 and we do not discuss it further in this paper. We describe the distribution of the data in Section 6 and conclude, with a view to the future, in Section 7.

2. SUMMARY OF COVERAGE

DR12 presents all of the data gathered by SDSS-III, which extended from 2008 August to 2014 June, plus a small amount of data gathered using the BOSS and APOGEE instruments in the first two weeks of 2014 July under the auspices of the next phase of the SDSS, SDSS-IV (see Section 7). The contents of the data release are summarized in Table 1 and described in detail in the sections that follow for each component survey of the SDSS-III.

As described in Section 4, the BOSS spectroscopy is now complete in two large contiguous regions in the northern and southern Galactic caps. DR12 represents a ~40% increment over the previous data release (DR10). The first public release of APOGEE data (Section 5) was in DR10; DR12 represents more than a three-fold increase in the number of spectra, and six times as many stars with 12 or more visits. In addition, DR12 includes the first release of data from MARVELS. MARVELS was in operation for four years (2008–2012); all resulting data are included in the release. The MARVELS data (Section 3) include ~5500 unique stars, most of which have 20–40 observations (and thus RV measurements) per star. DR11 and DR12 represent different pipeline processing of the

[140] http://www.sdss3.org/dr12
[141] http://www.sdss.org/dr12

Table 1
Contents of DR11 and DR12

	DR11		DR12	
	Total	Unique[a]	Total	Unique[a]
All SDSS Imaging and Spectroscopy				
Area Imaged[b] (deg^2)			31637	14555
Cataloged Objects[b]			1231051050	469053874
Total Spectra			5256940	L
Total Useful Spectra[p]			5072804	4084671
MARVELS Spectroscopy (Interferometric)				
Plates[c]	1581	241	1642	278
Spectra[d]	189720	3533	197040	5513
Stars with ⩾16 Visits	L	2757	L	3087
APOGEE Spectroscopy (NIR)				
Plates	1439	547	2349	817
Pointings	L	319	L	435
All Stars[e]	377812	110581	618080	156593
Stars observed with NMSU 1 m	L	L	1196	882
Commissioning Stars	27660	12140	27660	12140
Survey Stars[f]	353566	101195	590420	149502
Stars with S/N > 100[g]	L	89207	L	141320
Stars with ⩾3 Visits	L	65454	L	120883
Stars with ⩾12 Visits	L	3798	L	6107
Stellar Parameter Standards	7657	1151	8307	1169
Radial Velocity Standards	202	16	269	17
Telluric Line Standards	46112	10741	83127	17116
Ancillary Science Program Objects	20416	6974	36123	12515
Kepler Target Stars[h]	11756	6372	15242	7953
BOSS Spectroscopy (Optical)				
Spectroscopic Effective area (deg^2)	L	8647	L	9376
Plates[i]	2085	2053	2512	2438
Spectra[j]	2074036	1912178	2497484	2269478
All Galaxies	1281447	1186241	1480945	1372737
CMASS[k]	825735	763498	931517	862735
LOWZ[k]	316042	294443	368335	343160
All Quasars	262331	240095	350793	294512
Main[l]	216261	199061	241516	220377
Main, $2.15 \leqslant z \leqslant 3.5$[m]	156401	143377	175244	158917
Ancillary Spectra	154860	140899	308463	256178
Stars	211158	190747	274811	247216
Standard Stars	41868	36246	52328	42815
Sky	195909	187644	238094	223541
Unclassified Spectra[n]	132476	115419	163377	140533
SEGUE-2[b] Spectroscopy (Optical)				
Spectroscopic effective area (deg^2)			L	1317
Plates				229
Spectra	L	L	155520	138099
All Optical[o] Spectroscopy from SDSS as of DR12				
Total Spectra			4355200	

Table 1
(Continued)

	DR11		DR12	
	Total	Unique[a]	Total	Unique[a]
Total Useful Spectra[p]			4266444	
Galaxies			2401952	
Quasars			477161	
Stars			851968	
Sky			341140	
Unclassified[n]			200490	

[a] Removing all duplicates, overlaps, and repeat visits from the "Total" column.
[b] These numbers are unchanged since DR8.
[c] Number of plate observations that were successfully processed through the respective pipelines.
[d] Each MARVELS observation of a star generates two spectra. Unique is number of unique stars.
[e] 2155 stars were observed during both the commissioning period and the main survey. Because commissioning and survey spectra are kept separate in the data processing, these objects are counted twice in the Unique column.
[f] The statistics in the following indented lines include only those observations which met the requirements of being survey quality.
[g] Signal-to-noise ratio per half-resolution element >100, summed over all observations of a given star.
[h] Kepler stars were originally targeted by APOGEE under an ancillary program, but eventually became part of the main target selection.
[i] Repeated observations of plates in BOSS are from the Reverberation Mapping program (Shen et al. 2015a; including 30 observations of a single set of targets to study variability), several other ancillary programs, and several calibration programs.
[j] This count excludes the small fraction (~0.5%) of the observations through fibers that are broken or that fell out of their holes after plugging. There were attempted observations of 2,512,000 BOSS spectra.
[k] "CMASS" and "LOWZ" refer to the two galaxy target categories used in BOSS (Ahn et al. 2012). They are both color-selected, with LOWZ galaxies targeted in the redshift range $0.15 < z < 0.4$, and CMASS galaxies in the range $0.4 < z < 0.8$.
[l] This counts only quasars that were targeted by the main quasar survey (Ross et al. 2012), and thus does not include those from ancillary programs: see Section 7, Dawson et al. (2013), and Pâris et al. (2014).
[m] Quasars with redshifts in the range $2.15 < z < 3.5$ provide the most signal in the BOSS spectra of the Lyα forest.
[n] Non-sky spectra for which the automated redshift/classification pipeline (Bolton et al. 2012) gave no reliable classification, as indicated by the `ZWARNING flag`.
[o] Includes spectra from SDSS-I/II (DR7; Abazajian et al. 2009). Although the MARVELS interference spectra are in the optical range (5000 Å $< \lambda <$ 5700 Å), for convenience of labeling we here differentiate between the MARVELS data as "interferometric" and the original SDSS or BOSS spectrograph data as "optical."
[p] Spectra on good or marginal plates.

same observed MARVELS data. The MARVELS fields were selected to have >90 FGK stars with $V < 12$ and 30 giant stars with $V < 11$ in the SDSS telescope 3° diameter field of view. A set of pre-selection spectra of these fields, used to distinguish giants and dwarfs and thus refine the MARVELS target list, was taken by the SDSS spectrograph in 2008. The raw data from these observations were released as part of DR9. In DR12, we provide the outputs from custom reductions of these data.

While SDSS-III formally ended data collection at the end of the night of 2014 June 30, the annual summer maintenance shutdown at APO occurred 2014 July 14. The SDSS-III BOSS and APOGEE targeting programs were continued during these two weeks and are included in the DR12 release.

In addition, prototype and commissioning data were obtained during SDSS-III for the SDSS-IV Mapping Nearby Galaxies at APO (MaNGA) project (Bundy et al. 2015), which uses the BOSS spectrographs to measure spatially resolved spectra across galaxies. The raw data from these observations are included in DR12, but reduced data products (including kinematic and stellar population measurements) will be released only with the first SDSS-IV data release.

We also made a single fiber connection from the APOGEE instrument to the nearby New Mexico State University (NMSU) 1 m telescope at APO for observations when the APOGEE instrument was not being fed photons from the 2.5 m telescope. These observations of a single star at a time were taken to extend the range of the APOGEE-observed stars to brighter limits, providing improved calibration with existing observations of these stars (see Holtzman et al. 2015, for details). These data and the reductions are included in the standard SDSS-III APOGEE DR12 products and can be identified by the denoted source.

3. MARVELS

The MARVELS survey (J. Ge et al. 2015, in preparation) was designed to obtain a uniform census of RV-selected planets around a magnitude-limited sample of F, G, and K main-sequence, subgiant, and giant stars. This survey aimed to determine the distribution of gas giant planets ($M > 0.5$ $M_{Jupiter}$) in orbits of periods <2 years and to explore the "brown dwarf desert" over the mass range $13 < M < 80$ $M_{Jupiter}$ (Grether & Lineweaver 2006). Measuring these distributions requires a target sample with well-understood selection and temporal sampling. These science goals translated to observational plans to monitor 8400 stars over 2–4 years with RV accuracies of 10–50 m s^{-1} for $9 < V < 12$ mag for each of the 24 epochs per star. These RV accuracy predictions were estimated to be twice the theoretical photon-noise limit.

The MARVELS instrument (Ge et al. 2009), the W. M. Keck Exoplanet Tracker, uses an innovative dispersed fixed-delay interferometer (DFDI) to measure stellar RVs by observing the movements of stellar lines across the fringe pattern created by the interferometer. The wavelength coverage of the interferometer is 5000 Å $< \lambda <$ 5700 Å and it simultaneously observes 60 science fibers.

MARVELS RVs are differential measurements based on the shift of a star's fringing spectrum at the current epoch relative to one from the template epoch. For more details on the MARVELS program and DFDI instruments, see Erskine et al. (2000), Ge (2002), Ge et al. (2002, 2009), van Eyken et al. (2010), Eisenstein et al. (2011), and J. Ge et al. (2015, in preparation).

As described in Eisenstein et al. (2011), the original plan was to build two MARVELS spectrographs so as to capture 120 stars per exposure and a total sample of 11,000 stars. However, due to a lack of funding, the second spectrograph was not built, meaning that the total number of stars observed was about 5500. We unfortunately encountered significant challenges in calibrating the RV stability of the MARVELS instrument. These difficulties led us to end MARVELS observing as of the summer shutdown in 2012 July, so as to

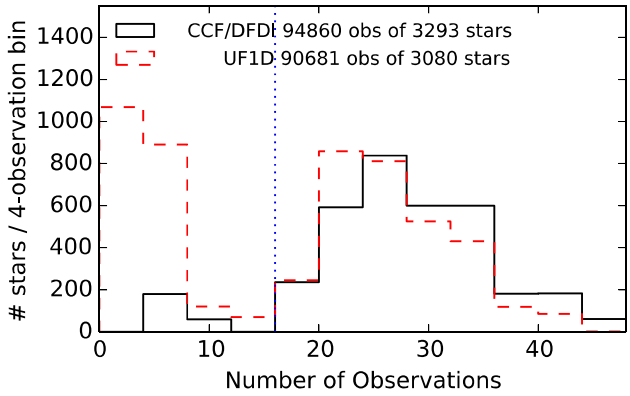

Figure 1. Distribution of the number of observations made of each MARVELS star that was processed by the CCF+DFDI (black solid) and the UF1D (red dashed) pipelines and met the respective quality cuts.

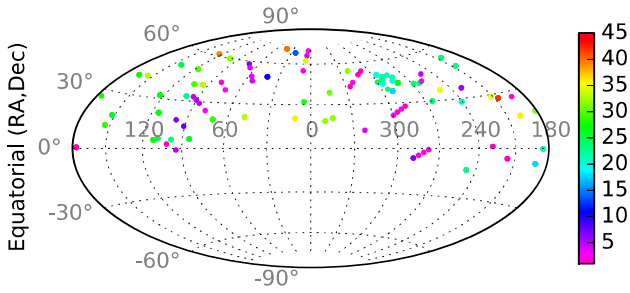

Figure 2. MARVELS sky coverage in equatorial coordinates. Each plate is plotted with a color coding giving the number of epochs the plate was observed.

focus on our data reduction efforts. For a detailed accounting and presentation of the observations see Table 1 and Figures 1 and 2. The typical rms scatter of the RV measurements in the data processing we have achieved to date has been three to five times greater than the photon noise limit. This increased rms has significantly limited the ability to discover planets in the MARVELS data. However, the distribution of rms values extends to near the photon noise limits and has led to cautious optimism that further improvements in processing and calibration may yield improved sensitivity to giant planets.

The original data processing pipeline was based on software from earlier DFDI prototype instruments (e.g., Ge et al. 2006). This pipeline used the full two-dimensional (2D) phase information, but the resulting RV measurements were limited to an rms of 100–200 $m\,s^{-1}$ by systematic instrumental variations. As described in detail below, the two RV estimates from this pipeline are presented in DR11 as the "cross-correlation function" (CCF) and DFDI reductions, with the latter explicitly incorporating the phase information from the interferometric fringes. These reductions revealed instrumental calibration variations that required a redesign of the analysis approach.

A subsequent reworked processing pipeline only analyzes the collapsed one-dimensional (1D) spectrum, without using the fringing information, but determines the calibration of the spectrograph dispersion on a more frequent basis (N. Thomas et al. 2015, in preparation). The results from this pipeline are presented in DR12 as the "University of Florida One Dimensional" (UF1D) reductions.

3.1. Scope and Status

MARVELS data collection began in 2008 October and ended in 2012 July. The majority of MARVELS stars were observed 20–40 times (Figure 1) with typical exposure times of 50–60 minutes. These exposure times were designed to reach a signal-to-noise ratio (S/N) sufficient to allow per-epoch RV precisions of tens of $m\,s^{-1}$ on stars of $7.6 < V < 12$ mag. The total number of observations was designed to enable the determination of orbital parameters of companions with periods between one day and two years without the need for follow-up RV measurements using additional telescopes. However, the problems in RV calibration, the shortened MARVELS observing period, and the fact that the second MARVELS spectrograph was never built meant that this ideal was not met for all targets. The observing was split into two two-year campaigns: Years 1+2: 2008 October—2010 December; and Years 3+4: 2011 January—2012 July. For any particular star, the time baseline between the first and last observation was thus typically 1.5–2 years.

During its four years of operation, MARVELS obtained 1565 observations of 95 fields collecting multi-epoch data for 5700 stars, with observations of 60 stars per target field.

While we provide all raw data and intermediate data products in this release, the CCF and DFDI results are limited to the 3533 stars with more than 10 RV measurements. The UF1D analysis results include 5513 stars from the 92 fields that pass the basic quality requirements of the pipeline. Restricting to stars with $\geqslant$16 observed epochs, which might be considered a reasonable threshold for searching for companions in the MARVELS data, yields 3293 stars in DR11 and 3233 stars in DR12 (a small number due to the somewhat tighter quality constraints).

3.2. A Brief Guide to MARVELS Data

Each spectrographic plate has two sets of 60 fiber holes, corresponding to two different fields to be observed in sequence. Both sets of fibers were plugged at the same time. In between observations of the two fields, the "gang" connector that joins the fibers from the cartridges to the long fibers that run to the MARVELS instruments was switched between the two sets of fibers.

A MARVELS exposure is the result of light from each of 60 fibers passing through a two-beam interferometer with one slanted mirror and then being dispersed in wavelength before being recorded on a 4k × 4k CCD. Thus, each MARVELS image contains 120 individual spectra as the beam-splitter produces two interference patterns for each star, one from each beam. The RVs for each star can then be calculated from a comparison of the fringing spectrum observations at different epochs.

In this data release, we provide the 2D raw images, the 2D slices of extracted spectra, the 1D collapsed spectra, and the calculated stellar velocities and associated observational metadata for each spectrum of each star and field.

3.3. Target Selection

Target selection for MARVELS is described in full in Paegert et al. (2015). We here summarize the key aspects of the

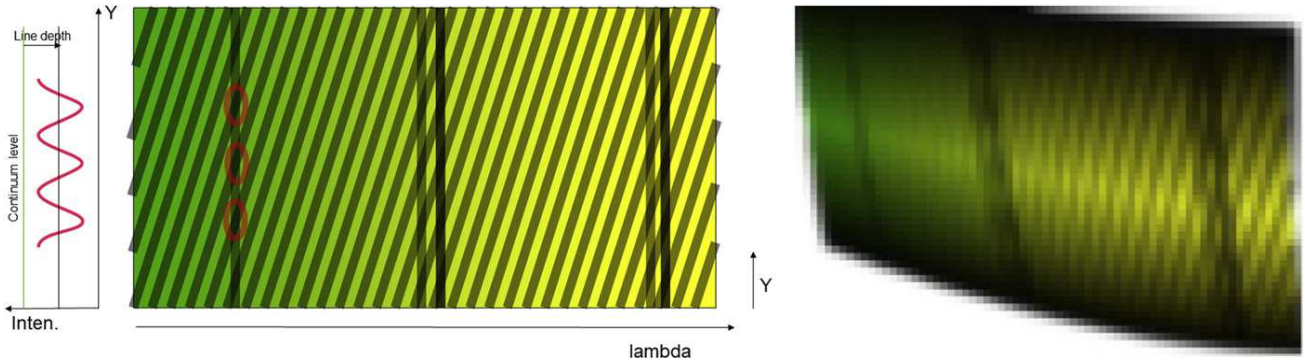

Figure 3. (Left) conceptual illustration of a portion of the spectrum of one star from MARVELS dispersed fixed-delay interferometry. For simplicity, we show only five absorption lines in this sample wavelength region; the full MARVELS wavelength range features thousands of absorption lines—most of these are blended at the MARVELS dispersion of R ~ 11,000. The diagonal pattern of constructive and destructive interference is not sharp as in this simple diagram, but rather varies sinusoidally with y. The phase of the best-fitting sinusoid to each column of the data determines the corresponding wavelength shift, given the slope of the interference comb. (Right) illustration of some of the real-world effects of variable projection of spectra onto the focal plane, spectrograph alignment, point-spread function, and the variable slope of the interference comb. Note the additional blending in each set of closely separated absorption lines. There are 120 of these spectra (each roughly 4096 pixels by 34 pixels) per MARVELS exposure.

MARVELS target selection in each two-year phase of the survey.

MARVELS aimed to have a target sample in the range of $8 < V < 12$ with a balance of 90% dwarf and subgiant stars with $T_{eff} < 6250$ K, and ~10% giant stars with $4300 < T_{eff} < 5100$ K (spectral types K2–G5). In the first two years of MARVELS, target selection was based on short "pre-selection" observations obtained with the SDSS spectrographs during the first year of SDSS-III to determine stellar surface temperatures and surface gravities. Because these observations used much shorter exposure times than standard SDSS observations, they were not automatically processed with the standard SDSS pipeline. Instead, the SDSS pipeline was used with some custom modifications to provide stellar spectra suitable for processing with the SEGUE Spectroscopic Processing Pipeline (SSPP; Lee et al. 2008). The raw data for these spectra were released as part of DR9. In DR12 we release these custom spectroscopic images, extracted spectra, and derived SSPP parameters as flat files, but due to their specialized and non-standard nature these have not been loaded into the CAS.

Unfortunately, the derived log g values—needed to discriminate giants from dwarfs—from these moderate-resolution spectra (R ~ 2000) were not reliable and the first two years of MARVELS targets resulted in a 35% giant fraction instead of the goal of 10%.

We thus employed a new method for giant-dwarf selection in Years 3 + 4. For this second phase of the MARVELS survey, temperature estimates were derived based on V − K and J − K colors following the infrared flux method of Casagrande et al. (2010), and giants were rejected based on a requirement of a minimum reduced proper motion (Collier Cameron et al. 2007) based on the measured 2MASS J-band proper motion together with the J-band magnitude and J − H color.

From 2011 January onward all MARVELS observations were carried out simultaneously with APOGEE, using plug plates drilled with holes for both sets of targets. The spectroscopic cartridges were adapted to allow connection of both the APOGEE and MARVELS fibers to the long fibers that run to the stabilized rooms that house the respective instruments. This joint observation mode yielded significant overall observational efficiencies, but imposed the restriction that both surveys observe the same fields with the same cadence. This shifted the MARVELS target fields much farther south than originally planned as APOGEE pursued observations toward the center of the Milky Way.

The sky distribution of all observed MARVELS fields is shown in Figure 2.

3.4. MARVELS Data Analysis

The MARVELS instrument is designed to be sensitive to wavelength shifts (and thus RV changes) in stellar spectra. It splits each input stellar spectrum into two beams, and then projects a slanted interference pattern of the recombined beams through a spectrograph (see Figure 3).

The dispersed slanted interference pattern effectively magnifies the resolution of a moderate-resolution spectrograph (R ~ 11,000) by translating wavelength shifts in the dispersion ("x") direction to much larger shifts in the "y" position. This slope is ~5 pixel pixel^{-1} for MARVELS. The design goal of the MARVELS analysis is to measure the shift of the interferometric sinusoid in the y direction to determine the wavelength offset due to a RV change.

The key challenges in the processing of MARVELS data are the calibration of the wavelength solution on the detector, identification and extraction of each spectrum, and the measurement of the slant of the interferometric comb and of the resulting interference pattern of the absorption-line features.

Our approach to analyzing the MARVELS data will be described in detail in N. Thomas et al. (2015, in preparation), which specifically describes the UF1D pipeline. The CCF +DFDI and UF1D pipelines follow many of the same steps, but differ in choices of calibration reference sources and complexity of model for instrumental variations. We here outline the important differences in the CCF+DFDI and UF1D processing.

3.4.1. Extraction of Spectra from the 2D Images

A key part of spectroscopic processing is determining the "trace," i.e., where the light from a given fiber target falls on the CCD. In an idealized instrument, the trace would lie horizontally along the CCD (constant y), and the light at a given wavelength would be distributed perpendicular to the trace (constant x), In practice, this is not true, and we correct

for these two according through a "trace correction" and "deslant correction."

The CCF+DFDI pipeline uses available Tungsten lamp continuum exposures with a diffuser to determine the trace of the spectrum on the CCD, and Thorium-Argon arc spectra to determine the deslant correction. The UF1D pipeline uses the Tungsten lamp exposures taken through an iodine cell to determine the trace, and the absorption lines in the observed stellar spectra to determine the deslant correction. The pipelines extract and correct 2D arrays for each spectrum based on their respective trace and deslant corrections.

3.4.2. Compression to 1D Spectra

The CCF+DFDI pipeline takes the 2D rectified spectrum and fits a sinusoid to the interference pattern along the y (slit) direction. The spectrum is then collapsed along y, and the resulting 1D spectrum plus sinusoidal fit parameters are stored. The combination of the collapsed spectrum and the sinusoidal fits is denoted a "whirl" in the provided CCF+DFDI data products.

The UF1D pipeline focuses on improvements to the instrumental calibration without adding complications from the details of the phase extraction. It simply collapses the 2D rectified spectra along the y direction to create 1D spectra, removing the information contained in the fringes. The UF1D pipeline was implemented as a step toward a new pipeline still in development that will include the more detailed calibration model used in the UF1D pipeline (see below) and will also make use of the phase information from the 2D spectra.

3.4.3. Characterizing the Instrumental Wavelength Drift

Determining the instrumental wavelength drift over time is critical in deriving reliable RV measurements. The instrumental drift is measured from calibration lamp exposures taken before and after each science frame. The calibration exposures are from a Tungsten lamp shining through a temperature-stabilized Iodine gas cell (TIO). This extracted spectrum is compared to that of the calibration lamp exposures taken on either side of the reference epoch chosen as the baseline for that star.

For the CCF+DFDI pipeline, the shift for each star was determined by comparing the extracted TIO spectrum to a single reference lamp spectrum taken on MJD 55165 (2009 November 29), and the measured RV for the star in question was corrected by the resulting offset. This correction attempts to express all changes in the instrument by a single parameter per fiber. The large variance in the resulting RVs has shown that this approach does not fully capture the complex nature of the calibration changes across the detector.

In an effort to capture the fact that the velocity offset may be a function of wavelength, the UF1D pipeline calculates a separate shift value for each 100 pixel chunk of each spectrum, corresponding to ~17 Å. The reference TIO pair for each field is chosen to be the one that brackets the observation with the highest stellar flux observations. These instrumental shift values are then used as corrections to each chunk of the spectrum before the stellar RV shifts are determined.

3.4.4. Measuring the Stellar RV Shifts

In CCF+DFDI, the stellar RV is measured by comparing the extracted stellar spectrum from a given stellar exposure to the spectrum at the template epoch. The template epoch is selected as the highest S/N observation available for the selected star. We first calculate the barycentric correction (due to the orbit of the Earth around the Sun) as part of the comparison with the template epoch, and then use cross-correlation to measure the RV offset of the 1D spectrum. This raw stellar RV shift is corrected for the instrumental drift determination from the previous step and labeled as the CCF measurement. The fringe shifts as a function of wavelength are then used to refine these velocity offsets to generate the final DFDI measurements. These two successive calculations are reported in separate tables in DR11 with CCF and DFDI suffixes in the name of the respective tables.

In principle, the DFDI RVs should be more precise. However, given the challenges in measuring stable RVs from the processing, we find it useful to compare the results with (DFDI) and without (CCF) the fringe corrections.

In UF1D, the pixel shift of each stellar spectrum with respect to that from the template date is determined for the same 100 pixel chunk based on a least-squares solution that minimizes the difference in values in each pixel, and then corrected for the calibration drifts measured from the TIO measurements. The resulting calibrated shifts are converted into a RV measurement by using a wavelength solution from each 100 pixel chunk to covert from pixel shift to wavelength shift to velocity shift. The outlier-rejected mean velocity shift across all 100 pixel chunks is then taken as the velocity shift for that spectrum for that epoch.

These RV shifts are then corrected for the barycentric motion of each observation. Because the RV measurements are all relative, the zero point of the RVs is meaningless, so the mean of all measurements for a given star is set to zero.

Because of the two-beam nature of the DFDI instrument, each star observation results in two spectra. These computations are done separately for each of these two spectra. The published data tables present RVs separately for each beam. To estimate the RV for the star on a given epoch one would in principle simply average the RVs from the two measurements. Because of the noticeable number of outliers in individual beam measurements, the use of an outlier rejection scheme is recommended.

3.5. Current Status and Remaining Challenges

As Figure 4 shows, the current data processing results in stellar RV variations of 50 m s^{-1} or larger even at high S/N, a value several times greater than that expected from photon statistics. This is mostly due to systematic uncalibrated wavelength shifts on timescales longer than a month; repeat observations of stars within the same lunation show much smaller RV variations. However, the figures show that some stars show rms radial velocity variations which approach the photon noise limit, suggesting that with proper calibration, the overall scatter should drop significantly. One possibility currently under investigation is that these stars represent specific fibers that are more stable, while the beams from other stars experienced greater hardware variation across repeated pluggings and fiber connections. Work continues on improving the analysis of the MARVELS data and our understanding of the long-term systematic effects.

Despite these challenges, the MARVELS DR11 reductions have been used to study low-mass and substellar companions (Fleming et al. 2012; Wisniewski et al. 2012; Ma et al. 2013), brown dwarfs in the "desert" (Lee et al. 2011), and exotic

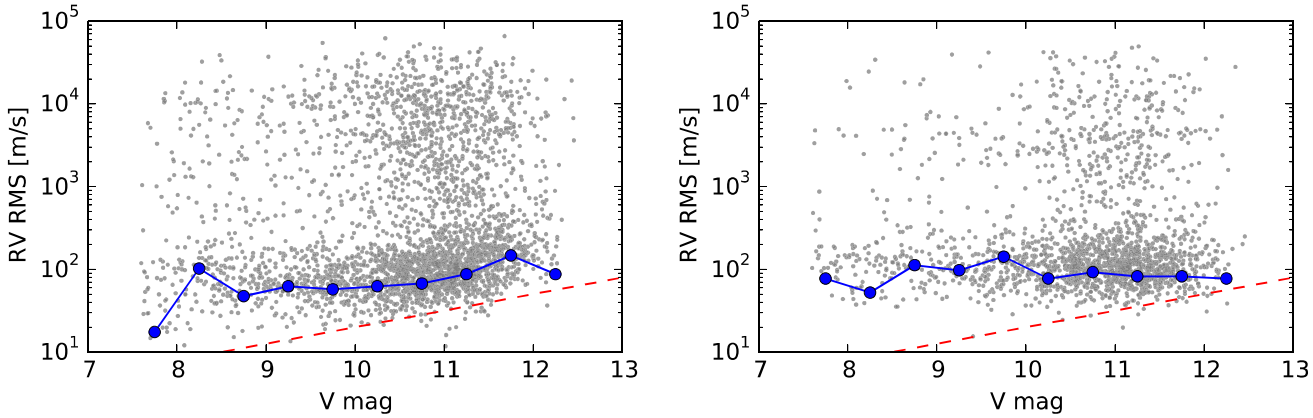

Figure 4. Distribution of rms of radial velocity measurements of MARVELS stars (gray points) for the DFDI (left) and UF1D (right) analyses, as a function of apparent magnitude. The mode of the rms in each 0.5 mag bin (blue circles and line) highlights the significant number of stars with rms near 50–100 m s^{-1}. However, a comparison with the theoretical photon limit (red dashed line) illustrates that the bulk of the rms values are many times higher than the limit. Despite this, there are stars whose radial velocity repeatability approaches the theoretical limit, suggesting that the large scatter for many of the observations is due to calibration problems, which might be improved with further development of the pipeline.

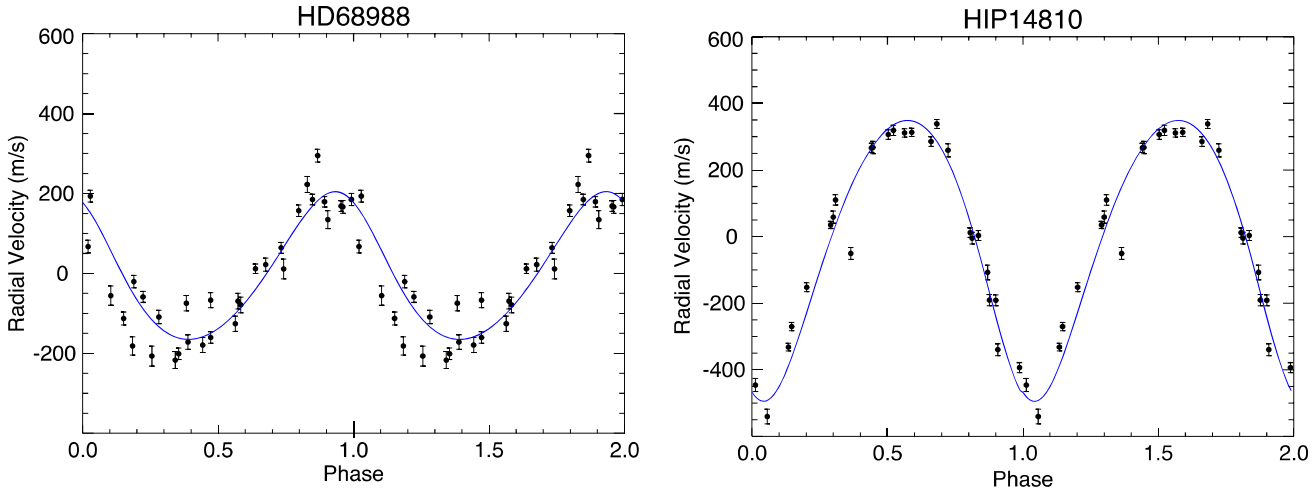

Figure 5. MARVELS observations of the radial velocities of the stars (left) HD68988 compared to the exoplanet model of Butler et al. (2006), and (right) HIP-14810 compared to the model of Wright et al. (2009). The phased data are shown over two periods for ease of visualization.

orbital systems (Mack et al. 2013). Figure 5 shows MARVELS RV measurements of two stars with known exoplanets, showing that MARVELS data are in good agreement with existing orbital models for these systems.

However, in general, the MARVELS data and analysis to date have not achieved the survey requirements for RV necessary to discover and characterize a fiducial 0.5-$M_{Jupiter}$ planet in a 100 day orbit. Figure 4 shows the achieved RV rms for the current pipelines as a function of stellar magnitude. The upper band of objects with rms from 1–10 km s^{-1} is predominantly true astrophysical variation from binary star systems. The distribution of objects with rms values in the range of 100 m s^{-1} is bounded near the photon limit, but the bulk lies several times above these limits.

4. BOSS

4.1. Scope and Summary

The BOSS main survey of galaxies and quasars over two large contiguous regions of sky in the northern and southern Galactic Caps was completed in Spring 2014. The majority of the galaxies were uniformly targeted for large-scale structure studies in a sample focused on relatively low redshifts ("LOWZ," with $z < 0.4$) and a sample with $0.4 < z < 0.7$ designed to give a sample approximately volume-limited in stellar mass ("CMASS"; B. Reid et al. 2015, in preparation). The total footprint is about 10,400 deg^2 (Figure 6); the value of 9376 deg^2 in Table 1 excludes masked regions due to bright stars and data that do not meet our survey requirements.

The main BOSS survey was completed in 2014 February. The additional dark time available through the 2014 summer shutdown was devoted to a portfolio of additional science programs designed to maximize the science return while taking advantage of the unique abilities of the SDSS system. Two of the largest such programs were a variability study of 849 quasars, designed to measure time delays between continuum and emission line variations ("Reverberation Mapping"; Shen et al. 2015a), and an early start on the planned cosmological studies with SDSS-IV (the Sloan Extended QUasar, ELG and LRG Survey, hereafter "SEQUELS," where "ELG" stands for "Emission Line Galaxy" and "LRG" stands for "Luminous Red Galaxy"), together with an exploratory set of plates to

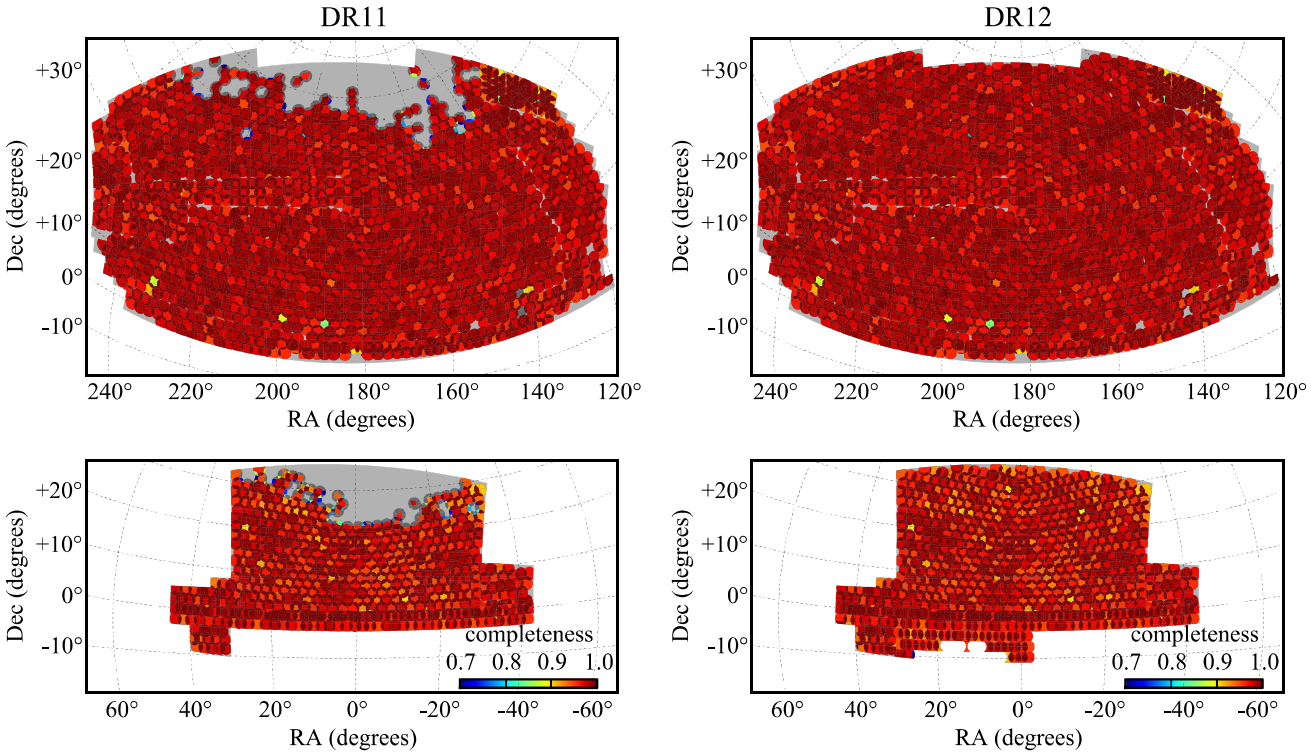

Figure 6. BOSS DR11 (left) and DR12 (right) spectroscopic sky coverage in the northern Galactic Cap (top) and southern Galactic Cap (bottom). The gray region (visible most clearly in the DR11 map) was the coverage goal for the final survey. The DR12 coverage map shows that we exceeded our original goals with a final total of 10,400 deg^2. The color coding indicates the fraction of CMASS galaxy targets that receive a fiber. The average completeness is 94% due to the limitation that no two fibers can be placed closer than 62″ on a given plate.

investigate the requirements for studies of high-redshift ELGs and other aspects of SDSS-IV. These and other BOSS ancillary programs executed since the DR10 release are described in Appendix.

4.2. Highlights from BOSS DR11

The DR11 and DR12 releases of BOSS data constitute increments of 35% and 47% in the number of spectra over DR10, respectively, processed using very similar pipelines. These increases were significant enough to warrant a new set of BOSS cosmological analyses for each of these releases. These key papers were one of the motivations for tagging a DR11 data set for later public release along with DR12. The cosmology analyses based on DR11 data include studies of isotropic galaxy clustering (Guo et al. 2015), anisotropic galaxy clustering (Samushia et al. 2014; Song et al. 2014; Sánchez et al. 2014; Gil-Marín et al. 2014a, 2014b; Beutler et al. 2014b; Reid et al. 2014), galaxy clustering in the LOWZ sample (Tojeiro et al. 2014), the baryon oscillations (BAO) in the clustering of the Lyα forest of distant quasars (Bautista et al. 2014; Delubac et al. 2015), the first detection of BAO in the cross-correlation between the Lyα forest and the quasars (Font-Ribera et al. 2014), an updated upper bound to the sum of neutrino masses (Beutler et al. 2014a), a summary BAO galaxy clustering analysis paper (Anderson et al. 2014b), and a joint cosmology analysis paper incorporating all of the BOSS cosmology constraints as well as those from Type Ia supernovae (SNe Ia) and anisotropies in the cosmic microwave background (Aubourg et al. 2014). The BOSS team plans a similar set of papers based on the full DR12 analyses.

4.3. Data Reduction Changes for DR12

The pipeline software for reduction of BOSS spectroscopic data was largely unchanged between DR10 and DR11. The classification and redshift-measurement aspects of this software are described in Bolton et al. (2012).

There were, however, some significant improvements to the spectrophotometric flux-calibration routine for DR12. These improvements were made to mitigate low-level imprinting of (primarily) Balmer-series features from standard-star spectra onto science target spectra. This imprinting was first documented in Busca et al. (2013) in observed-frame stacks of quasar continuum spectra. Although this effect is generally undetectable in any single-spectrum analysis, it has a small but non-negligible effect on the analysis of the Lyα forest across many thousands of quasar spectra. The change implemented for DR12 consists of a simple masking and linear interpolation of the flux-calibration vectors over the observed-frame wavelength ranges shown in Table 2. A more flexible flux-calibration vector model is retained at other wavelengths to accommodate real small-scale features in the spectrograph throughput. This more flexible model was necessary for the original SDSS spectrographs due to time variation in the dichroic filters, although it is likely unnecessary for the improved optical coatings on those surfaces in BOSS (see Smee et al. 2013).

In addition, we updated the pixel-response flats used to preprocess the spectrograph frames, improved the bias-subtraction code to catch and correct electronic artifacts that appear in a small number of frames, and updated the CCD bad-pixel and bad-column masks to reduce the incidence of corrupted but

Table 2
Wavelength Ranges Masked During BOSS Spectrophotometric Calibration

Line	Wavelength Range (Å)
Hò	3888.07 ± 25
[Ne III]	3969.07 ± 30
Hδ	4100.70 ± 35
Hγ	4339.36 ± 35
Hβ	4860.09 ± 35

Note. Observed-frame vacuum wavelength ranges that were masked and linearly interpolated during determination of spectrophotometric calibration vectors.

previously unflagged spectra. These changes reduce the number of corrupted spectra, and more accurately flag those that remain.

Table 3 gives the full history of significant changes to the BOSS spectrograph detectors and the calibration software to process its data since the BOSS survey began. See also Table 2 of Ahn et al. (2012) for additional changes to the hardware.

As in previous BOSS data releases, a unique tag of the `idlspec2d` spectroscopic pipeline software is associated with each unique sample of publicly released data.[142] Three tagged reductions of three separate samples are being released at the time of DR12. One (`v5_6_5`) is the "DR11" version that defines a homogeneous sample of BOSS data taken through Summer 2013; this is the version used in the cosmological analyses described in Section 4.2 above. A second label (`v5_7_0`) defines the main DR12 BOSS cosmological survey at its point of completion. A third tag (`v5_7_2`) is associated with the several extra observing programs undertaken with the BOSS spectrographs in Spring 2014 following the completion of the main BOSS survey program (Section 4.1, Appendix). These data-release software versions are summarized in Table 4.

Many of the pipeline changes for the ancillary programs involved bookkeeping and special cases for plates drilled with either fewer or more flux-calibration stars. In addition the SEQUELS plates targeted ELGs at high redshift, so the upper redshift limit of the galaxy template fitting (Bolton et al. 2012) was extended from $z = 1$ to $z = 2$. Thus DR12 includes several thousand SDSS galaxy spectra with tabulated redshifts above $z = 1$.

5. APOGEE

In this paper, we release both DR11 and DR12 versions of the APOGEE outputs, with considerably more stars (see Table 1) in the latter. The APOGEE release is described in detail in Holtzman et al. (2015). The DR11 parameters and abundances use the same version of the APOGEE Stellar Parameters and Chemical Abundances Pipeline (ASPCAP; A. E. García Pérez et al. 2015, in preparation) as in DR10. The DR12 version of ASPCAP is a major upgrade, in which abundances are determined for 15 individual elements. In addition, the DR12 ASPCAP code incorporated a number of technical improvements: multiple searches to avoid local minima in parameter space, new model atmospheres

[142] SDSS data processing software is publicly available at http://www.sdss.org/dr12/software/products/

Table 3
Significant Changes to the BOSS Spectrographs and the Data Reduction Pipeline

Date	MJD	Comments
2010 Apr 14	55301	R2 detector changed following electrical failure R2 pixel flat, bad pixel mask on all four cameras updated
2010 Aug	55410	Bad pixel mask updated on all four cameras Pixel flat updated on R1 and R2
2011 Aug	55775	R1 detector changed following electrical failure R1 pixel flat, bad pixel mask on all four cameras updated
2011 Oct 16	55851	R1 bad pixel mask updated
2012 Aug	56141	Bad pixel mask updated on all four cameras Pixel flat updated on R1 and R2
2013 Aug	56506	Pixel flat updated on R1 and R2
2013 Dec 23	56650	R2 detector had an electrical failure, but recovered R2 bad pixel mask and pixel mask updated
2014 Feb 10	56699	R1 pixel flat updated

Note. There are two BOSS spectrographs, each with a red and blue camera. Thus R2 refers to the red camera on the second spectrograph, which accepts light from fibers 501–1000. The August dates in the table above refer to the summer shutdowns.

Table 4
Spectroscopic Pipeline Versions Associated With Each BOSS Data Release

Data Release	Code Version	Comments
DR8	`L`	No BOSS spectroscopic data
DR9	`5_4_45`	First BOSS spectroscopic data release
DR10	`5_5_12`	Also includes data first released in DR9
DR11	`5_6_5`	Also includes data first released in DR10
DR12	`5_7_0`	Main BOSS sample, also includes data first released in DR11
DR12	`5_7_2`	Extra BOSS programs, non-overlapping with `v5_7_0`

with updated solar reference abundances and non-solar carbon- and α-element-to-iron abundance ratios (Mészáros et al. 2012), the use of a Gauss-Hermite function instead of a Gaussian to represent the instrumental point-spread function (PSF), and upgrades to the atomic and molecular line lists. These improvements do not change the derived fundamental stellar parameters systematically, but do improve their accuracy.

5.1. Scope and Summary

The APOGEE DR11 data include twice as many stars and spectra as DR10 (53,000 more stars and 200,000 more spectra), analyzed with the same pipeline. The APOGEE DR11 data have been used in several papers, including a determination of distances to and chemical abundances of red-clump stars (Bovy et al. 2014; Nidever et al. 2014), mapping of the Galactic interstellar medium using diffuse interstellar bands measured along the line of sight to APOGEE stars (Zasowski et al. 2015), and an identification of new Be stars and their H-band line profiles (Chojnowski et al. 2015).

APOGEE DR12 represents a further year of data and thus includes another 46,000 stars and 240,000 spectra over DR11. It also uses the updated analysis pipeline described above. The sky coverage of the final APOGEE DR12, covering the bulge, disk, and halo of our Galaxy is shown in Figure 7. The

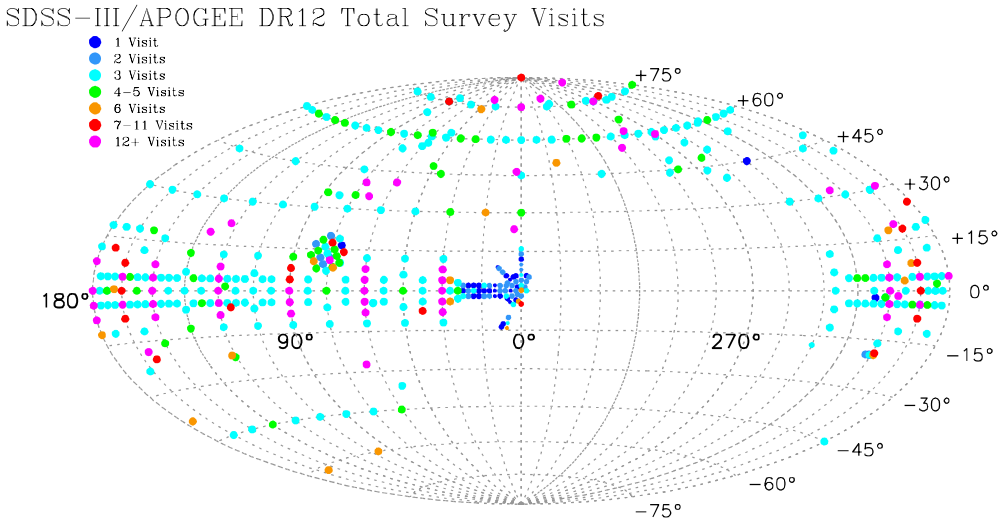

Figure 7. Sky coverage of APOGEE DR12 observations in Galactic coordinates. The number of visits to each field is denoted by the color coding from 1 visit (blue) through 12 or more visits (magenta).

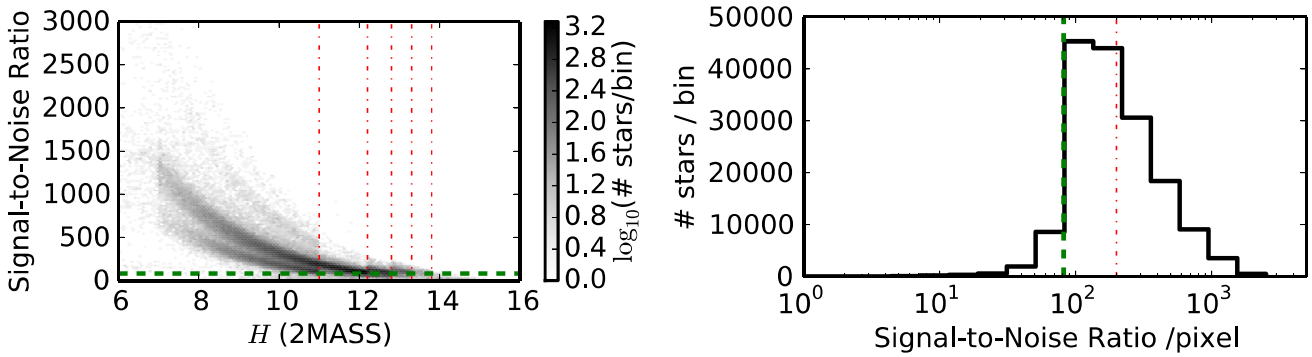

Figure 8. Distribution of S/N of APOGEE stars in DR12. With 1.5 pixels per effective half-resolution element, the science requirements goal of S/N ⩾ 100/half-resolution element is achieved with S/N ⩾ 82 pixel^{-1} (dashed green line). (Left) 2D histogram of S/N vs. 2MASS H magnitude. The red dashed–dotted lines denote the magnitude limits for the different bins of target brightness. The number of planned visits to APOGEE main targets was (1, 3, 6, 12, 24) visits for H < (11.0, 12.2, 12.8, 13.3, 13.8) mag. (Right) 1D histogram of S/N. The systematic floor in the effective S/N is ~200 (red dashed–dotted line).

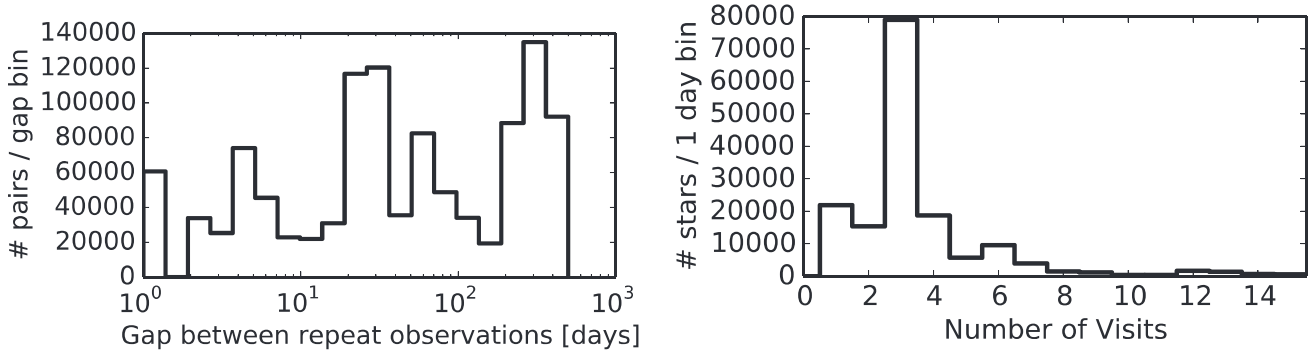

Figure 9. (Left) distribution of time intervals between observations of a given APOGEE target in DR12. (Right) distribution of number of visits for individual APOGEE targets in DR12.

additional observations of stars that already appeared in DR10 improve the S/N of these stars and also provide opportunities for studies of RV and other variations in the observed stellar spectra. Figure 8 demonstrates that we achieved our goal of S/N > 100 per half-resolution element for the APOGEE sample. Figure 9 shows the distribution of time baselines and the number of observations of each star.

A succinct overview of the APOGEE survey was presented in Eisenstein et al. (2011) and a full summary will be given by S. Majewski et al. (2015, in preparation). The APOGEE spectroscopic data processing is described in Nidever et al. (2015). The pipeline for deriving atmospheric parameters and abundances from the spectra will be described by A. E. García Pérez (2015, in preparation). The spectra, stellar

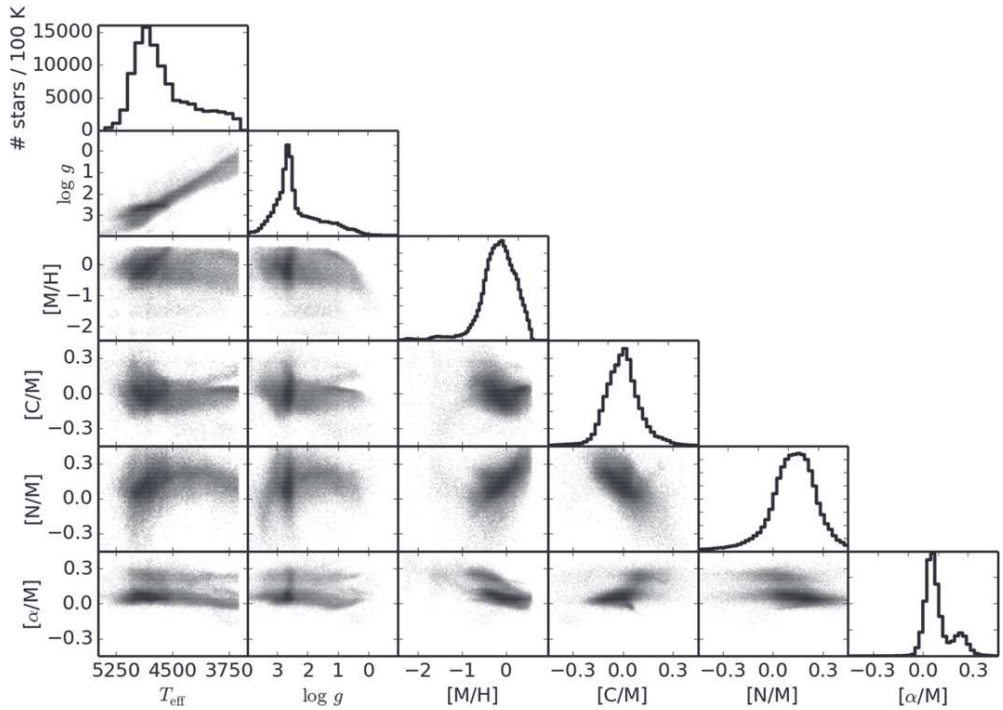

Figure 10. Key stellar parameters ($T_{\rm eff}$, log g) and key metallicity indicators ([M/H], [C/M], [N/M], [α/M]) for stars with APOGEE observations in DR12. These distributions are strongly affected by the selection of stars targeted for APOGEE spectroscopy. The gray scale is logarithmic in number of stars.

parameters, and abundances for DR11 and DR12 are described in Holtzman et al. (2015).

Figure 10 shows the observed distribution of the key stellar parameters and abundances for APOGEE DR12. Obtaining robust and calibrated values of $T_{\rm eff}$, log g, and [M/H] along with individual abundances for 15 elements has required development of new stellar libraries (Zamora et al. 2015) and H-band spectral line lists (Shetrone et al. 2015). After describing these fits, we discuss a value-added catalog of red clump stars, then describe specific target classes of APOGEE stars that are new since DR10.

5.2. Abundances of 15 Elements in APOGEE DR12

In DR12, we provide the best-fitting values of the global stellar parameters, as well as individual elemental abundances for C, N, O, Na, Mg, Al, Si, S, K, Ca, Ti, V, Mn, Fe, and Ni.

The spectra are fit to models based on spectral libraries from astronomical observations combined with laboratory and theoretical transition probabilities and damping constants for individual species. The final measurements and associated uncertainties are calibrated to observations of stellar clusters, whose abundance patterns are assumed to be uniform.

The abundances are most reliable for stars with effective surface temperatures in the range 3800 K $\leqslant T_{\rm eff} \leqslant$ 5250 K. For cooler atmospheres ($T_{\rm eff}$ < 3800 K), the strengths of molecular transitions are increasingly sensitive to temperature, surface gravity, molecular equilibrium, and other physical details, giving rise to a greater uncertainty in the inferred abundances. Stars with warmer atmospheres ($T_{\rm eff}$ > 5250 K) or at low metallicity ([Fe/H] $\lesssim -1$) have weaker lines, making it more difficult to measure abundances.

5.3. Red Clump Stars in APOGEE

This APOGEE data release also contains the DR11 and DR12 versions of the APOGEE red-clump (APOGEE-RC) catalog. Red clump stars, helium core-burning stars in metal-rich populations, are good standard candles, and thus can be used as a spatial tracer of the structure of the disk and the bulge. RC stars are selected using the log g, [Fe/H], and near-infrared colors available for each APOGEE star. The construction of the DR11 APOGEE-RC catalog and the derivation of the distances to individual stars were described in detail by Bovy et al. (2014). The DR11 catalog contains 10,341 stars with distances accurate to about 5%, with a contamination estimated to be $\lesssim$7%.

The DR12 RC catalog applies the same selection criteria to the full DR12 APOGEE sample, but re-calibrates the surface gravities to a scale appropriate for RC stars; the standard DR12 surface-gravity calibration is not appropriate for RC stars. The calibration starting from the uncalibrated outputs of ASPCAP for surface gravity, $\log g_{\rm uncal.DR12}$ is

$$\log g_{\rm RC} = 1.03\ \log g_{\rm uncal.DR12} - 0.370,$$

for $1 < \log g_{\rm uncal.DR12} < 3.8$ (outside of this range the $\log g_{\rm RC} - \log g_{\rm uncal.DR12}$ correction is fixed to that at the edges of this range). The DR12 APOGEE-RC catalog contains 19,937 stars with an estimated contamination $\lesssim$3.5% (estimated in the same manner as for the DR11 catalog, see Bovy et al. 2014).

5.4. Additional Target Classes in APOGEE DR12

Target selection for APOGEE was described in Zasowski et al. (2013). As with BOSS, the targets for APOGEE are dominated by uniformly selected samples designed to meet the

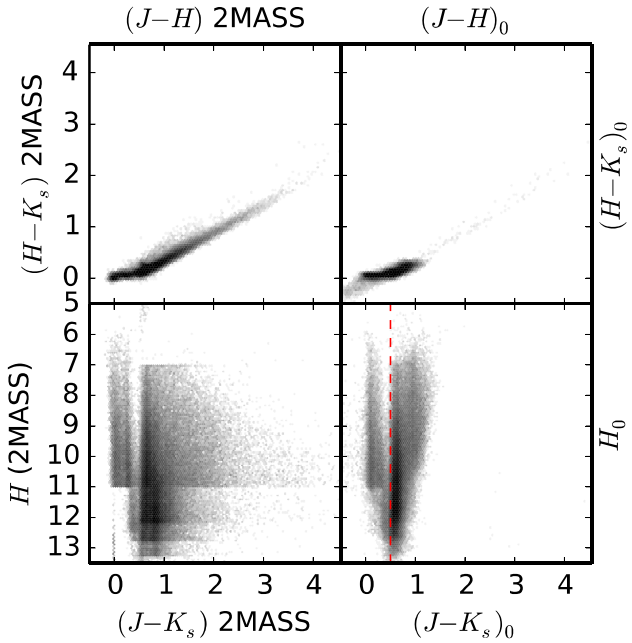

Figure 11. Near-infrared colors and H magnitudes of APOGEE targets as observed (left panels) and corrected for Galactic dust extinction (right panels). The vertical dashed line in the lower-right panel at $(J - K_s)_0 = 0.5$ mag indicates the selection cutoff for the main APOGEE red giant sample. Objects bluer than this line are from observations of telluric calibration stars, commissioning data, or ancillary program targets. The gray scale is logarithmic in number of stars.

key APOGEE science goals, but also feature additional ancillary programs to take advantage of smaller-scale unique science opportunities presented by the APOGEE instrument. The final distribution of 2MASS magnitudes and colors for all APOGEE targets are presented in Figure 11, both as observed, and corrected for Galactic extinction. Because many of the APOGEE target fields are at quite low Galactic latitudes, the extinction corrections can be quite substantial, even in the infrared.

Some of the additional dark time from the early completion of the BOSS main survey was used for the existing APOGEE main program, and allowed the addition and expansion of several ancillary science programs. DR12 adds four additional ancillary target classes to those described in Zasowski et al. (2013) and extends two previous ancillary programs. We briefly describe these additions here:

Radial Velocity Monitoring of Stars in IC 348. The "Infrared Spectroscopy of Young Nebulous Clusters" (IN-SYNC) ancillary program originally observed the Perseus sub-cluster IC 348. Subsequent to those observations a set of stars was targeted for further follow-up to (1) search for substellar companions in bright field stars of all spectral types; (2) search for stellar and substellar companions around low-mass M stars; (3) search for pre-main-sequence spectroscopic binaries in IC 348; (4) study a newly identified Herbig Be object (HD 23478/BD+31 649) and (5) enhance the completeness of the IC 348 sample with 40 additional targets. These 122 stars are labeled with APOGEE_TARGET2 bit set to 18.

Probing Binarity, Elemental Abundances, and False Positives Among the Kepler Planet Hosts. This ancillary project observed 159 Kepler Objects of Interest (KOI; e.g., Burke et al. 2014), 23 M dwarfs, and 25 eclipsing binaries, at high cadence (~21 observations), over a period of 8 months to study binarity, abundances, and false positives in the planet host sample. This project aims to detect stellar and brown dwarf companions of Kepler host stars, provide detailed abundances for several elements, and understand planet formation in binary systems. KOI targets were selected from the KOI catalog with $H_{Vega} < 14$; "eclipsing binary" targets were selected with $H < 13$, periods > 5 days, and classified as having a "detached morphology" as listed in the catalogs of Prša et al. (2011) and Slawson et al. (2011), plus two systems from Gaulme et al. (2013); and "M dwarf" targets were drawn from the catalog of Dressing & Charbonneau (2013) with $T_{eff} < 3500$ K and $H < 14$. These 208 stars are labeled with APOGEE_TARGET2 bit set to 19.

Calibration of the Gaia-ESO Spectroscopic Survey Program. A sample of 41 stars was observed to provide improved calibration of stellar parameters in conjunction with the Gaia-ESO Survey[143] (Pancino & Gaia-ESO Survey consortium 2012). These observations are labeled with the setting of APOGEE_TARGET2 bit 20.

Re-Observation of Commissioning Bulge Stars to Verify Radial Velocity Accuracy. A set of 48 stars in the bulge of the Milky Way that had originally been observed during the early commissioning phase of the APOGEE instrument was re-observed to provide a verification of the APOGEE RV estimates. These observations are labeled with the setting of APOGEE_TARGET2 bit 21.

In addition, two previous ancillary programs were expanded in DR12. The IN-SYNC ancillary program (APOGEE_TARGET2= 13) to study young stellar objects (YSO) in the Perseus molecular cloud (see Cottaar et al. 2014 and Foster et al. 2015 for more details) was expanded in DR12 to observe 2634 stars in the Orion A molecular cloud. The APOGEE ancillary program to observe Kepler stars for asteroseismology and stellar parameter calibration (APOGEE_TARGET1= 27) proved extraordinarily useful (e.g., Epstein et al. 2014) and was folded into the main APOGEE target selection for DR12.

6. DATA DISTRIBUTION

The data for DR11 and DR12 are distributed through the same mechanisms available in DR10, with some URL modifications to accommodate the ongoing transition to SDSS-IV and an associated unification of the SDSS web presence under the "sdss.org" domain. Raw and processed image and spectroscopic data are available through the Science Archive Server[144] (Neilsen 2008) and through an interactive web application.[145] The catalogs of photometric, spectroscopic, and derived quantities are available through the Catalog Archive Server[146] (Thakar et al. 2008; Thakar 2008a). More advanced and extensive querying capabilities are available through "CasJobs," which allows time-consuming queries to be run in the background[147] (Li & Thakar 2008). GUI-driven queries of the database are also available through SkyServer.[148] Links to all of these methods are provided at http://www.sdss.org/dr12/data_access. The data processing software for

[143] http://www.gaia-eso.eu/
[144] http://data.sdss3.org/sas/dr12
[145] http://dr12.sdss3.org
[146] http://skyserver.sdss.org/dr12
[147] http://skyserver.sdss.org/casjobs
[148] http://skyserver.sdss.org

APOGEE, BOSS, and SEGUE are publicly available at http://www.sdss.org/dr12/software/products. A set of tutorial examples for accessing SDSS data is provided at http://www.sdss.org/dr12/tutorials.

7. THE FUTURE: SDSS-IV

SDSS-IV began in 2014 July, as SDSS-III completed its observations. It will continue the legacy of SDSS with three programs on the 2.5 m Sloan Foundation Telescope to further our understanding of our Galaxy, nearby galaxies, and the distant universe.

The extended Baryon Oscillation Spectroscopic Survey (eBOSS; K. Dawson et al. 2015, in preparation) is obtaining spectra of LRGs over the redshift range $0.6 < z < 1.0$ and quasars in the range $0.9 < z < 3.5$ over 7500 deg^2, and ELGs from $0.6 < z < 1.0$ over 1500 deg^2, with an aim to measure the BAO peak to an accuracy of < 2% in four redshift bins. eBOSS also includes a spectroscopic survey (TDSS) of variable stars and quasars (the Time Domain Spectroscopic Survey; TDSS; E. Morganson et al. 2015, in preparation), along with a program to obtain optical spectra of X-ray selected sources (The SPectroscopic IDentification of ERosita Sources; SPIDERS). Many of the BOSS ancillary programs described in Appendix are exploratory or pilot studies to test aspects of eBOSS target selection.

SDSS-I/II established our understanding of galaxies in the $z \sim 0.1$ universe. The SDSS-IV Mapping Nearby Galaxies at APO (MaNGA) program (Bundy et al. 2015) will revisit 10,000 of these galaxies in far greater detail using integral-field fiber bundles to study spatially resolved galaxy properties, star formation, and evolution.

As Figure 7 makes clear, APOGEE has sampled only a fraction of the Milky Way, and has missed the southern skies completely. The APOGEE exploration of the Milky Way will continue with SDSS-IV. APOGEE-2 will use the existing spectrograph on the 2.5 m Sloan Foundation Telescope. In addition, a second APOGEE instrument will be built and installed on the 2.5 m du Pont Telescope at Las Campanas Observatory, Chile, providing an all-sky view of the Galaxy.

SDSS-IV will continue the sequence of SDSS public data releases, starting with a first release of spectroscopic data in 2016.

Data Release 12 marks the final data release of the SDSS-III project, which began development in 2006 and conducted six years of fully dedicated operations at APO. In total, SDSS-III collected 5200 deg^2 of ugriz imaging and about 3.4 million spectra. The total SDSS data set now contains over 5 million spectra, with connections to nearly all areas of astrophysics. The median extra-galactic redshift is now 0.5. We thank the full SDSS-III collaboration and partner institutions for their tremendous efforts toward the realization of the ambitious goals of the project, and we look forward to the many public uses of this vast legacy data set.

SDSS-III Data Release 12 has made use of data products from the Two Micron All-Sky Survey, which is a joint project of the University of Massachusetts and the Infrared Processing and Analysis Center/California Institute of Technology, funded by the National Aeronautics and Space Administration and the National Science Foundation.

SDSS-III Data Release 12 based APOGEE targeting decisions in part on data collected by the Kepler mission. Funding for the Kepler mission is provided by the NASA Science Mission directorate.

SDSS-III Data Release 12 based MARVELS targeting decisions in part on the Guide Star Catalog 2.3. The Guide Star Catalogue-II is a joint project of the Space Telescope Science Institute and the Osservatorio Astronomico di Torino. Space Telescope Science Institute is operated by the Association of Universities for Research in Astronomy, for the National Aeronautics and Space Administration under contract NAS5-26555. The participation of the Osservatorio Astronomico di Torino is supported by the Italian Council for Research in Astronomy. Additional support is provided by European Southern Observatory, Space Telescope European Coordinating Facility, the International GEMINI project and the European Space Agency Astrophysics Division.

SDSS-III Data Release 12 selected a significant number of BOSS ancillary targets based on data products from the Wide-field Infrared Survey Explorer, which is a joint project of the University of California, Los Angeles, and the Jet Propulsion Laboratory/California Institute of Technology, funded by the National Aeronautics and Space Administration.

SDSS-III Data Release 12 made use of Astropy, a community-developed core Python package for Astronomy (Robitaille & Tollerud 2013).

SDSS-III Data Release 12 made use of the Exoplanet Orbit Database and the Exoplanet Data Explorer at exoplanets.org.

SDSS-III Data Release 12 made use of the NASA/IPAC Extragalactic Database (NED) which is operated by the Jet Propulsion Laboratory, California Institute of Technology, under contract with the National Aeronautics and Space Administration.

SDSS-III Data Release 12 made use of data from Pan-STARRS1. The Pan-STARRS1 Surveys (PS1) have been made possible through contributions by the Institute for Astronomy, the University of Hawaii, the Pan-STARRS Project Office, the Max-Planck Society and its participating institutes, the Max Planck Institute for Astronomy, Heidelberg and the Max Planck Institute for Extraterrestrial Physics, Garching, The Johns Hopkins University, Durham University, the University of Edinburgh, the Queen's University Belfast, the Harvard-Smithsonian Center for Astrophysics, the Las Cumbres Observatory Global Telescope Network Incorporated, the National Central University of Taiwan, the Space Telescope Science Institute, and the National Aeronautics and Space Administration under grant No. NNX08AR22G issued through the Planetary Science Division of the NASA Science Mission Directorate, the National Science Foundation grant No. AST-1238877, the University of Maryland, Eötvös Loránd University (ELTE), and the Los Alamos National Laboratory.

Funding for SDSS-III has been provided by the Alfred P. Sloan Foundation, the Participating Institutions, the National Science Foundation, and the U.S. Department of Energy Office of Science. The SDSS-III web site is http://www.sdss3.org/.

SDSS-III is managed by the Astrophysical Research Consortium for the Participating Institutions of the SDSS-III Collaboration including the University of Arizona, the Brazilian Participation Group, Brookhaven National Laboratory, Carnegie Mellon University, University of Florida, the French Participation Group, the German Participation Group, Harvard University, the Instituto de Astrofisica de Canarias, the Michigan State/Notre Dame/JINA Participation Group, Johns Hopkins University, Lawrence Berkeley National Laboratory,

Table 5
Parallel BOSS Ancillary Programs

Primary Program	Sub-program	Bit Number	Number of Fibers[a]	Number of Plates
QSO Selection with WISE	QSO_WISE_FULL_SKY	10	26966	623
Hard X-Ray AGN	XMMSDSS	11	25	13
H_2O Maser Galaxies	IAMASERS	12	50	45
Binary Black Holes	DISKEMITTER_REPEAT	13	92	70
WISE BOSS	WISE_BOSS_QSO	14	20898	312
Quasar Pairs	QSO_XD_KDE_PAIR	15	628	273
Galaxy Cluster Spectroscopy	CLUSTER_MEMBER	16	2757	268
M Dwarf/Wide Binaries	SPOKE2	17	93	65
Census of Nearby Galaxies	PTF_GAL	19	173	107
QSO Spectrophotometry	QSO_STD	20	1458	158

[a] More precisely, this is the number of spectra in each ancillary program that were denoted as "specprimary," i.e., the best observation of a given object. For ancillary programs that involved repeated observations of objects previously observed in BOSS, the number in this column may differ from the number of actual fibers drilled for the program by < 1%.

Max Planck Institute for Astrophysics, Max Planck Institute for Extraterrestrial Physics, New Mexico State University, New York University, Ohio State University, Pennsylvania State University, University of Portsmouth, Princeton University, the Spanish Participation Group, University of Tokyo, University of Utah, Vanderbilt University, University of Virginia, University of Washington, and Yale University.

APPENDIX
TARGET SELECTION AND SCIENTIFIC MOTIVATION FOR BOSS ANCILLARY SCIENCE PROGRAMS

As described in Eisenstein et al. (2011) and Dawson et al. (2013), up to 10% of the BOSS targets were reserved for ancillary programs, i.e., those with scientific aims that went beyond those of the core quasar and galaxy samples.

Ancillary programs observed in the 2009–2010 and 2010–2011 seasons are documented in Dawson et al. (2013), and those observed in the 2011–2012 season were documented in Ahn et al. (2014). There were additional categories of ancillary programs included in the 2012–2014 observing seasons, which are released for the first time with DR12, and which we document here. In particular, BOSS completed observations of its uniform galaxy and quasar samples over the full footprint (Figure 6) several months before the end of SDSS-III observing, allowing a number of focused programs to be carried out.

All BOSS ancillary programs initiated after 2012 can be identified by having a non-zero ANCILLARY_TARGET2 bitmask. We present in this Appendix the scientific motivation for each program, the number of fibers assigned, and a description of the target selection algorithms. The labels for each target bit name appear in bold font in what follows. The new programs fall into three categories: those that are dispersed throughout the remainder of the BOSS footprint at low density ("parallel ancillary programs," Section A.1, Table 5), those that were located in small regions of sky at high density ("dedicated ancillary programs," Section A.2, Table 6), and those associated with a pilot survey in advance of eBOSS ("SEQUELS programs," Section A.3, Table 7). Most of the latter two categories were observed in the last six months of SDSS-III observations, after the main survey had been completed. Some of these programs are self-contained science projects in themselves, some represent calibrations or refinements of SDSS or BOSS spectroscopic programs, and some, like the SEQUELS programs, are preparatory for future surveys, especially eBOSS. While few of these programs have generated published results at this writing, a significant number of papers are in preparation which use these data. Note that there is often scientific or algorithmic overlap between many of the programs, reflecting the multiple calls for ancillary programs within the SDSS collaboration.

The selection algorithms in these different programs typically use PSF, model (for galaxy magnitudes), or cmodel (for galaxy colors; Abazajian et al. 2004) SDSS photometry, all corrected for Galactic extinction following Schlegel et al. (1998). Occasionally, fiber magnitudes are also used. The selection for many programs also uses photometry from the Wide-field Infrared Survey Explorer (WISE, Wright et al. 2010). WISE carried out a full-sky survey in four bands, centered at 3.6, 4.5, 12, and 22 μm; the resulting photometry (which is reported on a Vega system, unlike the AB system of SDSS) is referred to as W1, W2, W3, and W4, respectively, in what follows. We include the WISE catalog photometry of SDSS objects in both the DR11 and DR12 contexts in the CAS database. A number of programs use a reprocessing of the WISE data (Lang 2014) or forced photometry of WISE images at positions from SDSS (Lang et al. 2014).

A.1 BOSS Parallel Ancillary Programs

All new parallel ancillary target classes found in DR12 were given a priority lower than both the primary galaxy and quasar targets and previously approved ancillary programs. The targeted samples for these parallel ancillary programs are therefore not complete. We list these programs roughly in the order of the distance to the targets; in Table 5, we list them in bit order.

Characterizing Low-mass M Dwarfs Using Wide Binaries. M dwarf stars make up ~70% of the stars in the Galaxy by number and have lifetimes longer than the age of the universe. They are thus valuable tracers of the chemical and dynamical evolution of the Milky Way, but their complex spectra dominated by molecular bands make it difficult to determine their ages and metallicities. This program targets earlier-type binary companions to known M dwarf stars; these companions should share the same metallicity and age as the M dwarf but have atmospheres that are easier to interpret. These systems can be used to refine relations between M dwarf properties and

Table 6
BOSS Ancillary Programs with Dedicated Plates

Primary Program	Sub-program	Bit Number	Number of Fibers[a]	Plate ID
ELG with Deep Photometry	FAINT_ELG	18	2588	6931–6933
LRGs from SDSS and WISE	HIZ_LRG	21	8291	6373–6398
LRGs from SDSS and WISE	LRG_ROUND3	22	2543	6373–6398
Galaxy Incompleteness with WISE	WISE_COMPLETE	23	9144	6373–6398
TDSS/SPIDERS/eBOSS Pilot Survey	TDSS_PILOT	24	859	6369, 6783
TDSS/SPIDERS/eBOSS Pilot Survey	SPIDERS_PILOT	25	363	6369, 6783
TDSS/SPIDERS/eBOSS Pilot Survey	TDSS_SPIDERS_PILOT	26	107	6369, 6783
Variability-Selected Quasars	QSO_VAR_LF	27	2401	6370, 6780–6782
TDSS/SPIDERS/eBOSS Pilot Survey	TDSS_PILOT_PM	28	129	6783
TDSS/SPIDERS/eBOSS Pilot Survey	TDSS_PILOT_SNHOST	29	7	6783
eBOSS in CFHTLS	FAINT_HIZ_LRG	30	684	7027–7032
eBOSS in CFHTLS	QSO_EBOSS_W3_ADM	31	3517	7027–7032
Wide-Area XMM fields	XMM_PRIME	32	2422	7235–7238
Wide-Area XMM fields	XMM_SECOND	33	648	7235–7238
SEQUELS ELG	SEQUELS_ELG	34[b]	4884	7239–7243,7245–7248
Stars Across SDSS	GES	35	410	7330–7333, 7450–7453
Stars Across SDSS	SEGUE1	36	5262	7253–7256, 7454–7457
Stars Across SDSS	SEGUE2	37	2104	7253–7256, 7454–7457
Stars Across SDSS	SDSSFILLER	38	4710	7330–7333, 7450–7453
SEQUELS ELG	SEQUELS_ELG_LOWP	39[b]	3170	7239–7243,7245–7248
Orion and Taurus	25ORI_WISE	40	290	7261
Orion and Taurus	25ORI_WISE_W3	41	484	7261
Orion and Taurus	KOEKAP_STAR	42	252	7260
Orion and Taurus	KOE2023_STAR	43	202	7259
Orion and Taurus	KOE2068_STAR	44	276	7257
Orion and Taurus	KOE2023BSTAR	45	563	7259
Orion and Taurus	KOE2068BSTAR	46	602	7257
Orion and Taurus	KOEKAPBSTAR	47	542	7260
Stars Across SDSS	COROTGESAPOG	48	2	7258
Stars Across SDSS	COROTGES	49	47	7258
Stars Across SDSS	APOGEE	50	145	7258
Stars Across SDSS	2MASSFILL	51	324	7258
Orion and Taurus	TAU_STAR	52	734	7262
SEQUELS	SEQUELS_TARGET	53	L [c]	7277–7329, 7374–7429
Reverberation Mapping[d]	RM_TILE1	54	230	7338–7340
Reverberation Mapping[d]	RM_TILE2	55	619	7338–7340
Faint Quasars	QSO_DEEP	56	2484	7334–7337
Faint Quasars	LBG	57	168	7336–7337
LOFAR Sources	ELAIS_N1_LOFAR	58	410	7562–7565
LOFAR Sources	ELAIS_N1_FIRST	59	321	7562–7565
LOFAR Sources	ELAIS_N1_GMRT_GARN	60	356	7562–7565
LOFAR Sources	ELAIS_N1_GMRT_TAYLOR	61	1019	7562–7565
LOFAR Sources	ELAIS_N1_JVLA	62	56	7562–7565

[a] More precisely, this is the number of spectra in each ancillary program that were denoted as "specprimary," i.e., the best observation of a given object. For ancillary programs that involved repeated observations of objects previously observed in BOSS, the number in this column may differ from the number of actual fibers drilled for the program by < 1%.
[b] These targets are part of the SEQUELS program, described in Section A.3.
[c] SEQUELS targets are discussed in detail in Section A.3.
[d] These objects were observed over 30 epochs. All these objects have previous spectra, and thus none of these observations are designated as "specprimary."

spectral signatures (e.g., Stassun et al. 2008; Dhital et al. 2012).

Fibers denoted by the SPOKE2 target flag were assigned to candidate binary companions of spectroscopically confirmed low-mass stars in the Sloan Low-mass Wide Pairs of Kinematically Equivalent Stars (SLoWPoKES; Dhital et al. 2010, 2015) project. A previous ancillary program, the Low-Mass Binary Stars program (Dawson et al. 2013) consisted of systems with angular separations 65–180″. SPOKE2 extends that target sample to late-M spectral types, identifying binaries with separations between 3 and 20 arcsec. No proper motion requirement is imposed (Dhital et al. 2015). Targets have magnitudes in the range $17 < i_{PSF} < 21.3$.

A Census of Nearby Galaxies. We do not yet have a complete catalog of galaxies within 200 Mpc (Kasliwal 2011), hampering studies of nearby transients and the fine detail of the large-scale distribution of galaxies. The Palomar Transient Factory (PTF; Law et al. 2009) is performing a narrow-band survey in two filters, centered at 656 and 663 nm, to complete the catalog of galaxies in the local universe out to 200 Mpc. A sample of galaxies denoted by the PTF_GAL target flag was selected for spectroscopic confirmation. Galaxies without

Table 7
SEQUELS Targets

Sub-program	Bit Number	Number of Fibers[a]
DO_NOT_OBSERVE	0	L [b]
LRG_IZW	1	11778
LRG_RIW	2	11687
QSO_EBOSS_CORE	10	19461
QSO_PTF	11	13232
QSO_REOBS	12	1368
QSO_EBOSS_KDE	13	11843
QSO_EBOSS_FIRST	14	293
QSO_BAD_BOSS	15	59
QSO_BOSS_TARGET	16	L [b]
QSO_SDSS_TARGET	17	L [b]
QSO_KNOWN	18	L [b]
DR9_CALIB_TARGET	19	28602[b]
SPIDERS_RASS_AGN	20	162
SPIDERS_RASS_CLUS	21	1532
TDSS_A	30	9418
TDSS_FES_DE	31	42
TDSS_FES_DWARFC	32	19
TDSS_FES_NQHISN	33	74
TDSS_FES_MGII	34	1
TDSS_FES_VARBAL	35	62
SEQUELS_PTF_VAR	40	701
SEQUELS_COLLIDED	41	L

[a] More precisely, this is the number of spectra in an ancillary program that were denoted as "specprimary," i.e., the best observation of a given object. For ancillary programs that involved repeated observations of objects previously observed in BOSS, the number in this column may differ from the number of actual fibers drilled for the program by < 1%.
[b] These bits are not target classes, but are identifiers of quasars targeted by other algorithms satisfying various criteria, as described in the text.

known redshift were observed if they had an SDSS counterpart, a color $m_{656} - m_{663} > 0.7$ mag, and relatively blue broadband color as measured by SDSS ($g_{model} - i_{model} < 1.3$ mag). Images of all candidate galaxies were first visually inspected to avoid spurious detections.

Quasar Spectrophotometric Calibration. As described in Dawson et al. (2013) and Pâris et al. (2014), the fibers assigned to BOSS CORE and BONUS quasar targets (Ross et al. 2012) were offset in the focal plane to optimize throughput in the blue part of the spectrum, to better observe the Lyα forest. Because the standard stars are not observed with this same offset, the spectrophotometric calibration of these quasar targets is systematically incorrect. The QSO_STD flag denotes an additional sample of spectrophotometric standard stars, from 10 to 25 per plate spread evenly across the focal plane, that were drilled to follow the same offsets in the focal plane as the BOSS quasar targets. These objects are chosen using the same algorithm as for normal spectroscopic standard stars in BOSS, as explained in Dawson et al. (2013). Improved calibration gives improved measurements of quasar spectral energy distributions, important both for constraining quasar emission models, and for interpreting optical depth data in the Lyα forest (Lee et al. 2015).

Spectra of H_2O Maser Galaxies. One current route to the absolute calibration of the luminosities of SNe Ia as standard candles uses the 3%-accurate distance to NGC 4258 afforded by the well-studied H_2O maser in its center (Humphreys et al. 2013). Further improvements, by identifying other maser galaxies with supernovae, could decrease the uncertainty on local measurements of the Hubble Constant (Riess et al. 2011).

There is an apparent correlation between maser activity and host galaxy properties (Zhu et al. 2011); this correlation will be tested with spectroscopy of known maser host galaxies, and spectroscopy of SN Ia host galaxies will be used to identify plausible maser candidates. Targets, identified with the IAMASERS flag, were selected with no previous SDSS spectra and $i_{model} < 20$ mag. Objects targeted in the Bright Galaxies ancillary program (Dawson et al. 2013) were also removed from the IAMASERS target list.

Spectroscopy of Massive Galaxy Cluster Members. This program aims to obtain redshifts of candidate member galaxies of X-ray selected clusters. The sources are optical counterparts to X-ray clusters selected as faint sources in the ROSAT All-Sky Survey (Voges et al. 1999, 2000a) identified by applying the redMaPPer (Rykoff et al. 2014) cluster finding algorithm to the position of an X-ray source. The X-ray magnitude limit corresponds roughly to the brightest 30% of clusters that the X-ray satellite eROSITA will find within the BOSS area.

Objects denoted by the target flag CLUSTER_MEMBER are selected from the redMaPPer catalog with $i_{cmodel} < 19.9$ mag and $i_{fib2} < 21.5$ mag. Roughly 1000 candidate clusters were observed.

Repeated Spectroscopy of Candidate Close Binary Massive Black Holes. Second-epoch spectroscopy was obtained for SDSS I/II quasars that are candidate massive black hole binaries with separations less than 1 pc. The quasars were selected from the DR7 quasar catalog (Schneider et al. 2010) based on having double-peaked broad Balmer lines or significant velocity offsets between broad and narrow line centroids. The SDSS-III spectrum, identified by the DISKEMITTER_REPEAT target class, is separated from the first SDSS-I/II epoch by multiple years and provides a test of binarity by observing changes in the emission line properties. These data should allow new constraints on the close massive black hole binary population in SDSS quasars and will provide a better understanding of the nature of these peculiar broad-line profiles.

Spectroscopy of Hard X-ray Identified Active Galactic Nuclei. This sample, identified with the XMMSDSS target class, was designed to spectroscopically confirm hard (2–10 keV) X-ray selected AGN identified in the serendipitous XMM survey of SDSS(Georgakakis & Nandra 2011). These objects tend to lie at relatively low redshift, $z < 0.8$. Objects identified by the XMMSDSS target class were selected with f_X (2–10 keV)$> 4 \times 10^{-14}$ erg cm^{-2} s^{-1}and SDSS $r_{model} < 22$ mag. There was of order one target per square degree. The cross-correlation measurement of those AGN with the SDSS and BOSS galaxy samples will constrain the dark matter halo masses of X-ray AGN as a function of redshift and luminosity.

WISE BOSS: BOSS spectra of Mid-IR bright AGN: Photometry from the WISE All-Sky Data Release catalog was used in combination with SDSS photometry to select a 12 μm-flux-limited sample of quasars that goes beyond the main BOSS quasar sample (Ross et al. 2012). This allows studies of the completeness of the main quasar sample and an exploration of dust obscuration of quasars. The WISE_BOSS_QSO target class was selected as having $i_{PSF} < 20.2$, $W1 - W2 < 0.30$, $W1 < 2.0 + 0.667 g_{PSF}$, $r_{PSF} - W2 > 2.0$, $W2 < 18.5$, $W3 > 12.5$, and, for extended objects, $W3 > 10.3$. The resulting sample peaks at redshift $z \approx 1.4$.

Quasar Target Selection with WISE: This was a second sample of WISE-selected quasars, focused on the redshift range $z > 2.15$. Candidate quasars, identified with the QSO_WISE_FULL_SKY target class, were identified from SDSS photometry using an artificial neural network as described in Yèche et al. (2010). Point sources are assigned a photometric redshift estimate and a likelihood (NN) ranging from zero (stellar) to one (quasar). Objects with $NN > 0.3$ were considered targets if they were matched within 1.″5 of a WISE source, had color $i_{PSF} - W1 > 2.0 + 0.8(g_{PSF} - i_{PSF})$ and $i_{PSF} - W2 > 3.0$, and were brighter than $g_{PSF} = 21.5$ mag. These color cuts were designed to identify high-redshift quasars, and indeed almost 3/4 of the candidates have redshifts above 2. Objects satisfying this cut were assigned the QSO_WISE_FULL_SKY flag whether or not they were also targeted by the main BOSS quasar selection.

Quasar Pairs. Candidate quasar pairs separated by angles corresponding to less than a few hundred kiloparsecs were identified for spectroscopic confirmation. When combined with spectroscopy from other programs (e.g., Hennawi et al. 2006, 2010; Myers et al. 2008), this sample will provide a large statistical sample of quasar pairs necessary for small-scale clustering measurements. The target list consists of pairs of quasar targets selected using either the Kernel Density Estimation (KDE) method (Richards et al. 2009) or the XDQSOz method (Bovy et al. 2011). There are both low- and mid-redshift selection samples, both identified by the QSO_XD_KDE_PAIR target flag. The low-redshift selection includes targets with $g_{PSF} < 20.85$ mag and a matching target from the same selection within an angular separation, θ, of $1'' < \theta < 30''$. Objects are selected based on being in the XDQSOz low-redshift selection range ($0 < z < 2.2$) with probability being a quasar, $PQSO > 0.8$; or in the KDE catalog with flags indicating that the object is at low redshift and/or has an ultraviolet excess (`lowzts=1` or `uvxts=1`, as described in Table 2 of Richards et al. 2009).

The mid-redshift selection includes XDQSOz targets with $PQSO > 0.2$ that have a pair (from the same mid-z selection) within $1'' < \theta < 20''$. These targets are further culled to only retain pairs for which the product of the two XDQSOz probabilities for the pair integrated over $2.0 < z < 5.5$ is $PQSO_1 \times PQSO_2 > 0.16$. For both low- and mid-z selection, the following algorithm is implemented to clean the sample: (1) target all pairs where one or both of the objects in the pair are in a BOSS tiling overlap region; (2) for pairs where both objects are outside overlap regions, target the object with no existing spectrum; (3) for pairs where both objects are outside overlap regions and neither have existing spectra, target the fainter object; (4) discard all pairs where both objects are outside overlap regions and one of the pair is already a BOSS target; (5) discard all pairs where either object is a spectroscopically confirmed star or is obviously an artifact on visual inspection of the image; and (6) discard all targets (not pairs) that have an existing spectroscopic confirmation.

A.2 Ancillary Programs with Dedicated Plates

Because BOSS observations were proceeding ahead of schedule in 2012, a series of plates were added to the SDSS-III program to observe ancillary science programs. These plates do not have primary BOSS galaxy and quasar targets and instead consist entirely of ancillary science targets. The completeness of each dedicated sample is therefore typically higher than the completeness of the samples in the parallel ancillary programs. We describe each of these programs here, again sorted roughly by the distance of the targets. Table 6 summarizes the target categories, listed in order of ANCILLARY_TARGET2 bit. Note that a number of the programs include multiple target classes, each indicated by a separate bit.

Star Formation in the Orion and Taurus Molecular Clouds. This program obtained spectra of candidate YSO in the Orion and Taurus molecular clouds. The data provide a census of YSO into the brown dwarf regime, a measurement of the initial mass function at low masses, and a characterization of circumstellar disks as a function of stellar mass, extending previous studies to fainter magnitudes, to be sensitive to very low luminosity, low-mass objects. Objects were selected mostly from WISE photometry, as well as the 2MASS (Skrutskie et al. 2006) and Spitzer photometry (matching to SDSS imaging where available; Finkbeiner et al. 2004) in the Orion and Taurus regions. Objects were included to the detection limit of the WISE catalog, but those with $W1 > 7$ were removed to reduce contamination from luminous, very red, asymptotic giant branch stars. There are several target classes within this program, as detailed in Table 6.

The five plates in this program were designed in a heterogeneous manner due to the different availability of SDSS imaging in each field and the variation in the relative number of IR-excess sources. The latter is primarily related to the age of each star formation complex, as the circumstellar disk fraction decreases with stellar age. When limited SDSS photometry is available in a field, gri magnitudes are derived from the PPMXL/USNO-B1 catalog following the inverse of the transformations tabulated in Monet et al. (2003).

The 25 Ori spectroscopic plate targets WISE-detected stars within 1.5 degrees of the B3 star 25 Ori. It focuses on members of the young 25 Ori group and surrounding pre-main sequence stars in Orion and defines the target classes 25ORI_WISE and 25ORI_WISE_W3.

Objects were selected from the WISE catalog with detections in W1 and W3, with a magnitude limit of $W3 < 11.65$, and are assigned a target class of 25ORI_WISE_W3. Sources were required to be fainter than 15 in g, r, and i, and brighter than $g = 22$ and $i = 21$.

The remaining three Orion plates covering the Kappa Ori, NGC 2023, and NGC 2068 star formation regions were created in an identical manner and define the target classes KOEKAP_STAR, KOEKAPBSTAR, KOE2023_STAR, KOE2023BSTAR, KOE2068_STAR, and KOE2068BSTAR. For all three plates, objects in the *_STAR class are infrared excess sources selected by $W1–W2 > 0$ and a S/N in W1 greater than 10. The *BSTAR objects are other WISE detections within the field.

The Taurus spectroscopic plate targets objects with Spitzer mid-infrared 8 and/or 24 micron excess within 1.5 degrees of the center of the Taurus Heiles 2 molecular cloud. Our sample for Taurus focuses on very low-mass substellar objects with disks and edge-on disks which may have been mistaken for galaxies. The selection used IRAC1–IRAC4 > 1.5 and/or IRAC1–MIPS24 > 1.5 mag with S/N > 10 for IRAC1 and S/N > 7 for IRAC4 or MIPS24. Here IRAC1, IRAC4, and MIPS24 refer to Vega magnitudes measured through filters centered at 3.5, 8.0, and 24 microns on Spitzer. All science objects on the Taurus plate have a target class of TAU_STAR.

Stars Across the SDSS. This project aims to cross-calibrate the large spectral surveys which are giving us a detailed map of

the different stellar populations in the Milky Way. Dedicated stellar spectroscopic surveys such as SEGUE (Yanny et al. 2009), the RAdial Velocity Experiment (RAVE; Steinmetz et al. 2006), APOGEE, the Gaia/European Southern Observatory Survey (GES; Gilmore et al. 2012) and the massive Gaia survey itself (de Bruijne 2012) provide kinematic information and chemical diagnostics for large samples of stars. In addition, there are over 250,000 BOSS spectra of stars (Table 1), mostly targeted as quasar candidates. Derived stellar parameters, such as effective temperatures, surface graft's, and metallicities must be robust and consistent between surveys to use them jointly to build a coherent picture of our Galaxy. Because each survey targets a particular magnitude range, one must be careful to minimize systematic errors in stellar parameters as a function of distance.

This program obtained BOSS spectra of stars observed by the SEGUE1 and SEGUE2 surveys on eight plates (target classes SEGUE1, SEGUE2), GES targets in eight plates (target class GES), and one plate dedicated to stars from the COnvection, ROtation, and planetary Transit mission (CoRoT; Baglin 2002) also observed by GES and APOGEE (target classes COROTGES, COROTGETAPOG). As many CoRoT and GES stars were given fibers as possible, restricted only with the bright magnitude limit of $i > 14$ to avoid saturation in the spectrographs. There were not enough targets to fill all the fibers on the BOSS plates, particularly when the GES fields did not overlap with SEGUE-1 or SEGUE-2 plates, so the eight GES plates also targeted stars selected from the SDSS photometry (SDSSFILLER) with the following selection cuts to ensure good S/N and to avoid very cool stars for which it is more difficult to obtain accurate stellar parameters with the SSPP: $0 < g - r < 1.25$, $g < 19$, $i > 15$, $r > 15$. The CoRoT plate had targets chosen from APOGEE (target class APOGEE) and 2MASS (2MASSFILL) as well. Stars were targeted to sample the full parameter space of effective temperature, metallicity, and log g, as much as possible. The GES project (Milky Way survey) targeted stars with $0 < J - K < 0.7$, $12.5 < J < 17.5$, with near-infrared photometry from the Visible and Infrared Survey Telescope for Astronomy (VISTA; Emerson et al. 2004). In total, the eight GES plates gave spectra with high enough S/N for acceptable SSPP parameters for 296 stars with $-0.25 < g - r < 1.5$ and $14 < g < 19$.

A Galaxy Sample Free of Fiber Collisions. The finite size of the BOSS fiber ferrules means that no two fibers can be placed closer than 62″ apart on a given plate. These "fiber collisions" affect measurements of the small-scale clustering of galaxies from the CMASS and LOWZ samples. CMASS and LOWZ galaxies that were not observed in the main BOSS survey due to fiber collisions with other primary targets were added to ancillary target plates 6373–6398 (North Galactic Cap), 6780–6782 (on Stripe 82), 6369, and 6717. Fibers were also assigned to CMASS and LOWZ targets that suffered redshift failures (ZWARNING_NOQSO > 0; Bolton et al. 2012) in previous observations in the data reduction pipeline. These objects are identified with the CMASS or LOWZ target flags in the database; unlike all other objects discussed in this Appendix, they are not assigned a target class in ANCILLARY_TARGET2. This program significantly increases the completeness of these galaxy samples in the region covered by these plates and provides a useful data set for testing the fiber-collision correction methods that are currently used in BOSS clustering analyses (e.g., Guo et al. 2012). A total of 1282 targets were included in this program. These data have been used in an analysis of velocity bias in close pairs of galaxies by Guo et al. (2015).

Quantifying BOSS Galaxy Incompleteness with a WISE-Selected Sample. The CMASS sample is designed to select red galaxies of high stellar mass ($M_{stellar} > 10^{11}\,M_{\odot}$). This program (target class WISE_COMPLETE) aimed to explore a broader range of galaxy colors in the CMASS redshift range ($0.45 < z < 0.7$), using optical-IR cuts by combining SDSS and WISE. The sample criteria are $17.5 < i < 19.9$, $(r - W1) > 4.165$, and $i_{fib2} < 21.7$ (the latter uncorrected for Galactic extinction). Various quality flag cuts were imposed to limit spurious sources. Stars were eliminated using the SDSS morphological classifications for blue objects and a color–color cut in $(r - i, r - W1)$ space for red objects. A random subsample of 90% of these objects were selected as targets to meet the required target sky density.

Exploring $z > 0.6$ LRGs from SDSS and WISE. WISE and SDSS photometry was used to identify a sample of $z > 0.6$ luminous red galaxies, taking advantage of the fact that the 1.6 μm bump in old stellar populations (due to a local minimum in the opacity of the H^- ion) is redshifted into the WISE W1 band. This spectroscopic sample will be used to calibrate photometric redshifts in this range and to test target selection techniques for eBOSS.

Targets for this program were divided into a higher priority sample denoted HIZ_LRG and a lower priority sample denoted LRG_ROUND3. All objects were required to have

$$(i_{model} < 20.0 \,||\, z_{model} < 20.0) \,\&\&\, (z_{fib2} < 21.7 \,||\, i_{fib2} < 22.0).$$

Objects in the HIZ_LRG sample were selected to have

$$(r - i) > 0.98 \,\&\&\, (r - W1) > 2(r - i) - 0.5.$$

The LRG_ROUND3 sample used the same $r - W1$ cut, but the $(r - i)$ color cut was bluer, $(r - i) > 0.85$, in order to explore a broader range of galaxy colors.

Tests of eBOSS Target Selection in CFHTLS W3 Field. As a test of target selection algorithms to be used in eBOSS, six plates were dedicated to a selection of LRG and quasars at high density over a region of sky overlapping the Canada–France–Hawaii Telescope Legacy Survey (CFHTLS[149]) W3 imaging footprint.

Targets selected as potential galaxies in the redshift range $0.6 < z < 0.9$ were denoted FAINT_HIZ_LRG. These objects were selected in a similar manner to the targets that were assigned the HIZ_LRG flag described above, but at fainter magnitudes with a new tuning of color cuts. Targets were required to have

$$20 < z < 20.5, \left(z_{fib2} < 22.2 \,||\, i_{fib2} < 22.5\right),$$
$$(r - i) > 0.98, (r - W1) > 2(r - i).$$

Quasar targets, assigned the QSO_EBOSS_W3_ADM target class, were selected from photometry from CHFTLS, SDSS, and WISE, and variability data from PTF. Five selection techniques were applied, and all assigned the same target bit.[150] These selection criteria were as follows.

[149] http://www.cfht.hawaii.edu/Science/CFHTLS/

[150] The bit numbers in what follows are encoded in the bitmask W3bitmask, included in the file http://faraday.uwyo.edu/~admyers/eBOSS/ancil-QSO-eBOSS-W3-ADM-dr8.fits.

- Bit 0: W3 color box selection. These objects were selected from the CFHTLS W3 co-added catalog available at the TeraPix CFHT website.[151] The objects were restricted in CFHT magnitudes to $g < 22.8$. Stars were excised with the following color cuts (using CFHT photometry):

$$(g - r) - 0.5(u - g) < -0.2||$$
$$(g - r) + 0.7(u - g) < 0.6.$$

  The targets were required to be classified as point sources by SDSS and to have SDSS r magnitudes in the range $17 < r < 22$.

- Bit 1: SDSS XDQSOz selection. These objects were selected using the XDQSOz selection of Bovy et al. (2012) based on SDSS photometry. Point sources with $17 < r < 22$ were required to have an XDQSOz probability of being a quasar greater than 0.2.
- Bit 2: SDSS-WISE selection. This program used WISE forced photometry at SDSS source positions (Lang 2014; Lang et al. 2014). A stacked flux was created in SDSS gri (m_{opt}; with a relative (g, r, i) weighting of (1, 0.8, 0.6)), and a stacked flux was created in WISE W1 and W2 (m_{wise}; with (W1, W2) relative weights of (1, 0.5)). Objects were selected with $17 < m_{opt} < 22$, $(g - i) < 1.5$, and $m_{opt} - m_{wise} > (g - i) + 3.0$. Extended sources were allowed; the sample was restricted to sources with a difference between SDSS PSF and model magnitudes less than 0.1.
- Bit 3: CFHTLS Variability selection. Using three years of repeated observation in the one square degree field D3 of CFHTLS, objects were selected based on the variability measured in their light curves. Objects were selected on χ^2 and structure function parameters A and Γ (Palanque-Delabrouille et al. 2011) averaged over the three bands gri. Using colors c1 and c3 defined as in Fan (1999): $c1 \equiv 0.95(u - g) + 0.31(g - r) + 0.11(r - i)$ and $c3 \equiv -0.39(u - g) + 0.79(g - r) + 0.47(r - i)$, two selections were applied. The first used only CFHT information, requiring $A > 0.08$, $\chi^2 > 10.0$, $\Gamma > 0.3$, $c3 < 0.6 - 0.33c1$, and $g < 23.0$. The second used both CFHT and SDSS, and required that $A > 0.08$, $\chi^2 > 10.0$, $\Gamma > 0.2$, $g < 22.0$, and that the object be classified as point-like by SDSS.
- Bit 4: PTF variability selection. Using light curves computed from PTF R-band imaging linked to SDSS r with a color correction, quasar candidates were again selected by variability. All structure function or color-term parameters are defined as above (cf., Bit 3). The objects were required to have $A > 0.05$, $\chi^2 > 10.0$ and $\Gamma > 0.1$. In addition, the objects were limited to $g < 22.5$ and had to pass either of the following two criteria based on SDSS photometry: a color and magnitude cut $r > 18$ and $c3 < 1.0 - 0.33c1$, or a color and morphology cut requiring the object to be classified as point-like by SDSS and to have a probability of being a quasar greater than 0.1 according to the XDQSO algorithm.

eBOSS ELG Target Selection with Deep Photometry. This program used deep photometric data to select ELG candidates, to assess algorithms for eBOSS. Photometry extending to fainter limits than SDSS was used to assess algorithms for selection of Emission Line Galaxies (ELG) for spectroscopic observations. In particular, blue star-forming galaxies in the redshift range $0.6 < z < 1.2$ were selected from the CFHTLS Wide W3 field photometric redshift catalog T0007[152] (Ilbert et al. 2006; Coupon et al. 2009). Targets with the FAINT_ELG target class were selected at a density of nearly 400 objects per square degree, and three plates were observed centered on the same position. The sample was defined to help evaluate the completeness of the targeting sample and redshift success rates near the faint end of the ELG target population.

Selected objects satisfied the constraints:

$$20 < g < 22.8, -0.5 < (g - i) < 2 \text{ and}$$
$$-0.5 < (u - r) < 0.7(g - i) + 0.1.$$

All photometry was based on CFHTLS MAG_AUTO magnitudes on the AB system. Objects with known redshift were excluded. These data are described in Comparat et al. (2015), which measured the evolution of the bright end of the [O II] emission line luminosity function.

The TDSS/SPIDERS/eBOSS Pilot Survey. This program carried out pilot observations in two fields for two components of the SDSS-IV eBOSS survey: TDSS and SPIDERS (Section 7). The first field encompasses the existing XMM-Newton Large Scale Survey (XMM-LSS), deep multi-band CFHTLS field imaging, and a Pan-STARRS1 (PS1; Kaiser et al. 2002, 2010) medium deep survey field (MD01) with hundreds of epochs. The second field is also a PS1 medium deep field (MD03) located in the Lynx/IfA Deep Field. Both fields have 3–4 times as many PS1 epochs as does SDSS Stripe 82 (Annis et al. 2014), and PS1 continued monitoring these fields at the time the BOSS spectroscopy of these plates was carried out. There were five target selection algorithms on these plates, as follows:

Objects with the TDSS_PILOT target class were selected from PS1 photometry calibrated as described in Schlafly et al. (2012). Targets were selected by variability within each of the gri filters, with the requirement of a median PS1 magnitude $17 < mag_x < 20.5$ and at least 30 observed epochs within that filter. Objects were required to be point-like in SDSS, with the difference between PSF and model magnitude less than 0.05 in each filter, and with no detectable proper motions.

Lightcurves for objects that pass a variability threshold in at least one filter following Kim et al. (2011) were visually inspected in all three filters.

We assign each object a priority based on the number of passed criteria summed over filters, the source brightness, and whether or not a BOSS spectrum already exists.

Objects identified TDSS_PILOT_PM were selected the same way, but this identifier marks objects with significant ($>3\sigma$) total proper motion as measured by SDSS.

Objects identified TDSS_PILOT_SNHOST showed transient behavior in extended objects in the PS1 medium deep photometry, as described in Chornock et al. (2013).

Objects identified SPIDERS_PILOT were selected as X-ray sources with clear optical counterparts in SDSS DR8 imaging. The X-ray selection was performed on a source catalog constructed from public XMM-Newton data in the XMM-LSS area following the procedure described in Georgakakis & Nandra (2011). The sample was flux-limited in soft X-rays

[151] http://T07.terapix.fr/T07/Wide/W3/Big-Merged/W3_fusion_sm2.cat

[152] http://www.cfht.hawaii.edu/Science/CFHTLS/

(0.5–2 keV) to the expected limit of the eROSITA deep field survey ($\sim 6 \times 10^{-15}$ erg cm^{-2} s^{-1}), and were required to have $17 < r_{PSF} < 22.5$ and not to have been spectroscopically observed by BOSS as of DR9. Objects with higher soft X-ray flux were given higher priority in fiber assignment.

Objects targeted by both the SPIDERS and TDSS algorithms were given higher priority and were assigned the TDSS_SPIDERS_PILOT target class.

Follow-up spectroscopy of wide-area XMM fields. Like the SPIDERS program above, this program targeted X-ray-selected AGN from the XMM-XXL field, now using the full range of sensitivity from 0.5 to 10 keV. SDSS optical counterparts to X-ray sources were identified via the maximum-likelihood method (Georgakakis & Nandra 2011). The main spectroscopic target sample was selected to have $f_X(0.5\text{–}10\,\mathrm{keV}) > 10^{-14}$ erg cm^{-2} s^{-1} and $15 < r < 22.5$, where r is the PSF magnitude in the case of optical unresolved sources or the model magnitude for resolved sources. Targets in this sample are denoted XMM_PRIME. Secondary targets are sources with $f_X(0.5\text{–}10\,\mathrm{keV}) < 10^{-14}$ erg cm^{-2} s^{-1} and $15 < r < 22.5$, or radio sources selected in either 325 or 610 MHz from the catalog of Tasse et al. (2008). These targets are denoted XMM_SECOND.

Multi-Object Reverberation Mapping. The broad emission lines in AGN spectra can have flux variations correlated with variation in the continuum, but with a time delay interpreted as the mean light-travel time across the broad-line region. Measuring this time delay ("reverberation mapping") allows one to study the structure and kinematics of the broad-line regions of AGN. 849 spectroscopically confirmed quasars were observed over 30 epochs to study the variability of this sample.

The observations were scheduled with a cadence of four to five days, as weather allowed, with a goal of five epochs per month between 2014 January and the end of 2014 June. The typical exposure times were 2 hr for this program, and thus the final data from this program comprise a 60 hr effective exposure time for the targets in this field. The survey is described in Shen et al. (2015a).

Previous spectroscopy of the PS1 Medium Deep Field MD07 $(\alpha, \delta) = (213.^\circ704, +53.^\circ083)$ provided redshifts of roughly 1200 quasars in the redshift range $0 < z < 5$ over the area of a single plate. The sample was limited to quasars with $i < 21.7$. Lower-redshift quasars (whose time delay should be easier to measure) were given higher priority, and are indicated with the RM_TILE1 target class; essentially all of these were assigned a fiber. Higher-redshift targets (RM_TILE2) were tiled with the remaining fibers.

Three plates containing identical science targets were drilled at varying hour angle to ensure that the field was visible for six months. Each plate was given the normal number of sky fibers (80) but was allocated a substantially larger number of standard star fibers (70 rather than 20) to allow more rigorous tests of spectrophotometric calibration.

Early science results from these data include measurements of the velocity dispersions of the host galaxies of low-redshift quasars from the high S/N co-added spectra (Shen et al. 2015b), rapid trough variability in broad absorption line quasars (Grier et al. 2015), and the structure functions and time delays of a number of quasars.

Variability-selected Quasars at $1 < z < 4$ to $g = 22.5$. The QSO_VAR_LF bit labels a target class designed for studies of the quasar luminosity function to $g < 22.5$. The sample is located in Stripe 82 at $36° < \alpha < 42°$ where multi-epoch SDSS photometry is available, thus enabling a variability selection with the neural network presented in Palanque-Delabrouille et al. (2011). Targets with point-like morphology that passed a loose variability criterion were selected (neural network threshold of 0.5, where 1/0 indicates a quasar-like/stellar-like light curve). Extended sources which satisfied the color selection $c3 < 0.6 - 0.33c1$, where c1 and c3 are linear combinations of SDSS ugriz bands as defined in Fan (1999), were targeted if they passed a tighter variability criterion (threshold of 0.9).

Note that targets previously spectroscopically identified as quasars were not included in the sample and therefore do not have the QSO_VAR_LF bit set, even if they pass the selection criteria for this program.

Faint End of the Quasar Luminosity Function. Targets that have the QSO_DEEP bit set used the same variability selection as for QSO_VAR_LF, but were selected in the range $22 < g < 23.5$ from SDSS Stripe 82 data.

Slightly extended objects with $-0.15 < (r_{PSF} - r_{model}) < 0.15$ were selected to a neural network threshold of 0.9.

Additional targets were included in the sample when they had a large probability of being a quasar according to the KDE (Richards et al. 2009). Unresolved objects with $\mathrm{KDE}(1.0 < z < 2.2) \geqslant 0.999$ or slightly resolved objects with $-0.05 < (r_{PSF} - r_{model}) < +0.05$ and $\mathrm{KDE}(z > 2.2) \geqslant 0.985$ were included. Targets previously spectroscopically identified as quasars were not included in the sample and therefore do not have the QSO_DEEP bit set even if they pass the selection criteria.

Finally, a sample of candidate Lyman-Break Galaxies was selected in color-space and assigned the LBG bit. These targets are slightly extended objects that lie in one of two color box regions: $0 < (g - r) < 0.15$ && $(u - g) > (g - r) + 0.2$, or $0 < (g - r) < 1.0$ && $(u - g) > (g - r) + 1.25$.

SDSS-III Observations of LOFAR Sources. This ancillary program was intended to target radio sources identified in deep observations of the ELAIS-N1 region by the Low Frequency Array (LOFAR; van Haarlem et al. 2013). LOFAR observations were planned with the high-band antenna (HBA: 110–250 MHz) for roughly 10 hours over 9 deg^2 to eventually reach an rms depth of 100 μJy at 150 MHz. Spectroscopic confirmation of these sources will provide insight into the nature of the LOFAR radio population and aid in the science exploitation of new radio surveys. The LOFAR ELAIS-N1 region is well-studied by optical surveys and contains deep Jansky Very Large Array (JVLA) and Giant Metre-Wave Radio Telescope (GMRT) imaging data near the center of the field.

The LOFAR sample goes considerably deeper near the center of the spectroscopic field, concentrating the targets there and making it impossible to assign sky fibers uniformly over the focal plane. Instead, there were a large number of fiber bundles that did not contain a sky fiber and the usual sky interpolation routine in the automated BOSS reductions could not be applied to the four plates designed for this program. For these plates, the data reduction pipeline was modified to apply a constant sky model across each spectrograph (i.e., fibers 1–500 and 501–1000, respectively). This results in larger sky residuals than the typical calibrated BOSS spectra. With this in mind, users of these data should treat the automated redshift classification and narrow emission lines with caution.

All LOFAR radio sources were matched to SDSS optical counterparts found within 2″ of the radio source position. The SDSS position was used for the fiber placement. The target classes selected for this program are as follows:

ELAIS_N1_LOFAR targets were selected from a preliminary image of the ELAIS-N1 HBA data (115 to 190 MHz) that reached an rms noise level of 333 μJy. Approximately 800 sources were detected to a threshold of 1650 μJy and an additional 400 sources were detected to a threshold of 1000 μJy. These sources are distributed over a field of radius approximately 3° for a total surface area of roughly 30 $\deg^{-2}$. In addition, 387 fainter LOFAR sources that could be clearly identified by eye in the ELAIS-N1 field were targeted.

ELAIS_N1_FIRST sources lacked a detection by LOFAR but appeared in the catalog of the Faint Images of the Radio Sky at Twenty cm (FIRST) survey (Becker et al. 1995), and had an SDSS optical counterpart with $r_{model} < 23.0$. Fibers were placed at the SDSS position.

ELAIS_N1_GMRT_GARN sources were identified from deeper GMRT data at 610 MHz (rms depth of 40–70 μJy) from the Garn et al. (2008) source catalog. These sources are expected to be dominated by AGN.

ELAIS_N1_GMRT_TAYLOR targets were also selected from GMRT data (Taylor et al. 2014), which are even deeper (rms depth of 10 μJy) than that used in the ELAIS_N1_GMRT_GARN sample. The deep GMRT radio catalog includes 2800 sources over 1.2 $\deg^2$. The positional accuracy from the radio data appears to be better than 0.″5.

ELAIS_N1_JVLA sources were also selected to be much fainter than the other samples. The deep JVLA radio catalog includes 483 sources over 0.13 $\deg^2$ at an angular resolution of 2.″5 and rms noise of 1 μJy (Taylor et al. 2014). The positional accuracy is similar to the ELAIS_N1_GMRT_TAYLOR sample. Both this sample and the ELAIS_N1_GMRT_TAYLOR sample should include a significant fraction of star-forming galaxies at $z < 1$.

A.3 The Sloan Extended Quasar, ELG, and LRG Survey (SEQUELS)

SEQUELS serves both as a pilot program for the eBOSS survey of SDSS-IV and as a stand-alone science program within SDSS-III. SEQUELS also encompasses two SDSS-IV sub-programs to obtain spectra of variability-selected objects and X-ray detected objects, which are pilot studies for the TDSS and SPIDERS programs within eBOSS described in Section 7.

The main SEQUELS footprint lies in the North Galactic Cap. Targets were selected over the region covering $120° < \alpha < 210°$ and $45° < \delta < 60°$ within the nominal BOSS footprint, but only 300 $\deg^2$ of this area were observed. The targets in the primary SEQUELS program have the SEQUELS_TARGET bit set in the ANCILLARY_TARGET2 bitmask. Plates that were drilled but not observed before DR12 will be observed as part of eBOSS.

SEQUELS targets fell into four broad categories, which we describe in detail below: (1) luminous red galaxies (LRG), designed to extend the BOSS CMASS redshift coverage, yielding a median redshift of ~0.72; (2) quasars both as direct tracers of the cosmic density field at redshifts $0.9 < z < 2.2$, and as probes of the Lyα forest; (3) X-ray targets as a SPIDERS precursor, and (4) variability-selected targets as a TDSS precursor. Several other target classes do not fall neatly into any of these categories and are listed at the end.

In addition, SEQUELS incorporated a pilot program to identify high-redshift ELGs. The ELG targets are listed with the ANCILLARY_TARGET2 bitmask (Table 6). The bitmasks for all other SEQUELS programs are listed in Table 7 and are described in detail in what follows. Note that some of these bits (such as bit 0, DO_NOT_OBSERVE) do not indicate programs per se, but rather give information about the target selection process.

A.3.1 LRGs in SEQUELS

Target selection of LRGs in SEQUELS was designed to target massive red galaxies at $z \gtrsim 0.6$, using a combination of SDSS imaging and WISE photometry. The SDSS photometry (all model magnitudes corrected for Milky Way extinction) uses a new set of calibrations using a combination of PanSTARRS-1 (Kaiser et al. 2010) and SDSS stellar photometry (Finkbeiner et al. 2014). The residual systematics are reduced from 1% in griz (Padmanabhan et al. 2008) to 0.9, 0.7, 0.7, and 0.8% in the griz bands, respectively. In addition, some poorly constrained zero-points with errors exceeding 3% in the DR9 data are now significantly improved. This new photometry will be included in a future data release. The WISE photometry (now converted to the AB system) is forced photometry on SDSS positions (Lang et al. 2014).

There are two target classes focused on LRG; roughly 1/3 of the LRG objects are targeted by both. Both classes are magnitude limited to $z < 19.95$ and $i > 19.9$. The bright limit ensures that there is no overlap with the BOSS CMASS selection. Objects flagged LRG_IZW in the SEQUELS bitmask satisfy the color cuts $(i - z) > 0.7$ and $(i - W1) > 2.143(i - z) - 0.2$. Objects flagged LRG_RIW satisfy $(r - i) > 0.98$, $(r - W1) > 2(r - i)$, and $(i - z) > 0.625$; the latter cut pushes the sample to higher redshift.

A.3.2 Quasars in SEQUELS

The main sample of SEQUELS quasars is assigned the QSO_EBOSS_CORE target class and is designed to meet the eBOSS sky density goal of ~70 $0.9 < z < 2.2$ quasars $\deg^{-2}$.

The target selection makes no attempt to filter out higher-redshift quasars, so objects from this sample will also be useful for Lyα forest studies. Quasars in the CORE are selected by a combination of XDQSOz (Bovy et al. 2012) in the optical and a WISE-optical color cut, as detailed in A. Myers et al. (2015, in preparation); see also the description of bit 1 and 2 of the QSO_EBOSS_W3_ADM target class above. This sample (and all the SEQUELS quasar candidates which follow, unless otherwise indicated) are restricted to objects classified as point sources, with faint-end magnitude cuts of $g < 22$ or $r < 22$.

We also selected quasars via their variability as measured by the PTF; these are given the target class QSO_PTF. This sample is less uniformly selected, given the availability of multi-epoch PTF imaging, but that is acceptable for Lyα forest studies. These objects are limited in magnitude to $r > 19$ and $g < 22.5$.

Targets that have the QSO_EBOSS_KDE bit set in SEQUELS consisted of all objects from the KDE catalog of Richards et al. (2009) that had `uvxts=1` set (indicating that they had a UV excess, and thus were likely to be at $z \lesssim 2.2$) within that catalog. Only KDE objects that matched to a point source in the DR9 or the custom SDSS photometry used to select SEQUELS targets were included.

The QSO_EBOSS_FIRST bit indicates quasars that are targeted in SEQUELS because there is an SDSS source within 1″ of a source in the 2013 June 05 version[153] of the FIRST point source catalog (Becker et al. 1995).

An object is flagged QSO_BOSS_TARGET if it has been previously observed by BOSS and does not have either LITTLE_COVERAGE or UNPLUGGED set in the ZWARNING bitmask (see Table 3 of Bolton et al. 2012). Similarly, an object from SDSS DR8 is flagged QSO_SDSS_TARGET if it is included in the SDSS DR8 spectroscopic database, and similarly has neither of those flags set in ZWARNING.

We separately flagged those quasars with QSO_KNOWN whose spectra had been visually confirmed, as listed in the SDSS sample used to define known objects in BOSS (see Ross et al. 2012), and a preliminary version of the DR12 BOSS quasar catalog of I. Paris et. al. (2015, in preparation).

As part of SEQUELS, we also re-observed a number of high-redshift ($z > 2.15$) quasars that had low S/N spectroscopy in SDSS DR7 or BOSS, to improve the measurement of the Lyα forest.

Objects flagged QSO_REOBS had $0.75 \leqslant$ S/N/pixel < 3 in BOSS. This target class also included objects which have a high probability of being quasars based on their photometry, but had no signal in the BOSS spectra because of dropped fibers or other problems.

In the same spirit, BOSS spectra of some objects are of low enough quality that their classification as quasars, or measurements of their redshifts, are uncertain upon visual inspection. Such objects are designated as QSO? or QSO_Z? in the DR12 quasar catalog (I. Paris et. al. 2015, in preparation). Those objects in the SEQUELS footprint are re-observed, and given the QSO_BAD_BOSS target class. A preliminary, but close-to-final version of the DR12 catalog was used to define this sample for SEQUELS.

We set a flag bit, DO_NOT_OBSERVE, to indicate which previously observed quasars should not be re-observed, even if they were selected by one of the SEQUELS algorithms. It is determined by the following combination of target flags:

```
(QSO_KNOWN||QSO_BOSS_TARGET||QSO_SDSS_TARGET)
  &&
  !(QSO_BAD_BOSS||QSO_REOBS).
```

SEQUELS targeted quasars were selected in both the DR9 imaging used for BOSS and an updated DR12 imaging calibration intended for use in eBOSS targeting. The DR9_CALIB_TARGET bit signifies quasars that were selected for SEQUELS using the DR9 imaging calibrations instead of (or as well as) the updated DR12 imaging.

A.3.3 SPIDERS Targets within the SEQUELS Program

The goal of the SPIDERS program within eBOSS is to obtain SDSS spectroscopy for large samples of X-ray selected AGN and member galaxies of X-ray selected clusters. Two SPIDERS pilot programs were executed within SEQUELS using pre-eROSITA X-ray survey data.

SPIDERS_RASS_AGN targets are candidate AGN detected in the ROSAT All-Sky Survey (RASS). A parent sample of X-ray sources was formed from the concatenation of all Bright and Faint RASS catalog (Voges et al. 1999, 2000b) detections lying within the SEQUELS footprint. Given the large RASS positional uncertainties, we determine the most probable optical counterpart for each RASS source using a novel Bayesian algorithm (M. Salvato et al. 2015, in preparation), an extension of the method introduced by Budavári and Szalay (2008) applied to all SDSS photometric objects with $17 < r < 22$ within 1′ of each RASS detection. The algorithm uses the positional offset between each possible association, the positional errors, and the colors of the sources, given priors from a sample of previously matched XMM-Newton sources (Georgakakis & Nandra 2011). Identified sources which already had SDSS/BOSS spectra, were associated with objects in the Véron-Cetty and Véron (2010) cataloge of known AGN, or were associated with bright stars from the Tycho-II catalog (Høg et al. 2000), were removed.

Objects of type SPIDERS_RASS_CLUS are selected from the RedMapper catalog (Rykoff et al. 2014) of cluster members with $17.0 < i_{fiber2} < 21.0$ that lie in the SEQUELS footprint. A prioritization scheme penalizes lower richness clusters and favors highly ranked members in the photometric red sequences. We also targeted 22 clusters selected in XMM-Newton observations by the XCLASS-RedMapper survey (Clerc et al. 2012; Sadibekova et al. 2014) with richness (i.e., number of candidate members) greater than 20. The high-quality XMM-Newton data allows more detailed characterization of the cluster mass once the spectroscopic redshift is known (via, e.g., derivation of intra-cluster gas temperatures). Moreover, the identification of these objects as clusters is unambiguous given their X-ray data, so no cut is made on optical richness.

A.3.4 TDSS Targets within the SEQUELS Program

The TDSS program targeted variable objects matched between imaging in both Pan-STARRS1 and SDSS. There are two classes of TDSS targets: single-epoch spectroscopy (SES) and few-epoch spectroscopy (FES).

Single-epoch spectroscopy. These targets comprise the main body of TDSS targets and are flagged with target class TDSS_A.

We match SDSS point sources with $16 < i_{psf} < 21$ to the PS1 "uberCal" database of 2013 September, restricting to objects with more than 10 detections across the PS1 griz bands. We also eliminate sources with a $g < 22$ neighbor within 5″ or an $i < 12$ neighbor within 30″ to avoid problems with deblending issues.

To identify variables within this subsample, we use a three-dimensional KDE. We train our algorithm on known variables, using the Stripe 82 variable catalog from Ivezić et al. (2007) and require that the amplitude of variation in the g, r and i-bands be greater than 0.1. Our catalog of non-variables is taken from the Ivezić et al. (2007) standards catalog. We improve the purity of the latter catalog by requiring that our non-variables have at least eight SDSS observations in Stripe 82 and a reduced χ^2 relative to a model of no variability of less than 2 in the g, r and i bands. We require that variables, standards and candidates have SDSS and PS1 magnitude errors of less than 0.1 and at least two PS1 detections in three of the four bands in common between PS1 and SDSS bands (g, r, i and z).

Across the 3–4 qualified bands (as described above), we use the median PS1-SDSS magnitude difference (corrected photometrically so that it is 0 for a typical star), median PS1-only variability (essentially the variance minus the average error squared) and median SDSS magnitude as the three dimensions of our KDE. We bin and convolve both our variable and standard population within this space and define "efficiency" as

[153] http://sundog.stsci.edu/first/catalogs/readme_13jun05.html

the fraction of variables divided by the fraction of standards in every region of that space. We then use the PS1-SDSS difference, PS1 variability and median magnitude to assign an efficiency to every source in our sample.

We limit ourselves to sources with SDSS $i_{fib2} < 21$, and fainter than 17 in u, g and r fiber magnitudes. This removes potentially saturated sources. We also remove targets that already have SDSS or BOSS spectroscopy.

Few-epoch spectroscopy. These target bits represent FES programs that explicitly seek repeat spectra for objects of interest in order to monitor spectroscopic variability. The TDSS_FES program targets are as follows.

1. TDSS_FES_DE: Quasar disk emitters. These targets are quasars with $i < 18.9$ and broad, double-peaked or asymmetric Balmer emission line profiles, such as those in Strateva et al. (2006) ($z < 0.33$ for Hα and Hβ) and higher-redshift analogs from Luo et al. (2013) ($z \sim 0.6$ for Hβ and Mg II). This program seeks to characterize the variability of the broad emission line profiles, especially changes in asymmetry and velocity profiles, for comparison to models of accretion disk emission in the presence of asymmetries and/or perturbations.
2. TDSS_FES_DWARFC: Dwarf carbon stars (dCs). Most targets were chosen from the compilation of Green (2013) from SDSS spectroscopy. Objects were required to have significant (more than 3σ) proper motion (≈15 mas yr^{-1}) between the Palomar Observatory Sky Survey and SDSS photometry, ensuring that they are nearby, and thus likely to be dwarf stars. Observations of RV variations will identify binaries, thus testing the hypothesis that these stars became carbon-rich due to mass transfer from an asymptotic branch star via either wind accretion or Roche lobe overflow.
3. TDSS_FES_NQHISN: This program targets $z < 0.8$ DR7 quasars with high S/N spectra to study broad-line variability on multi-year timescales.
4. TDSS_FES_MGII: This program targets quasars that showed evidence for temporal velocity shifts in the Mg II broad emission lines in previous repeat SDSS spectroscopy (Ju et al. 2013) in order to look for evidence of super-massive black hole binaries.
5. TDSS_FES_VARBAL: These objects are selected from the Gibson et al. (2008) broad absorption line quasar catalog, to look for variability in the absorption troughs. Further description of this program can be found in Filiz et al. (2012, 2013).

A.3.5 Other Target Classes in SEQUELS

Galaxies from the main BOSS target selection, both LOWZ and CMASS, that were not assigned fibers due to fiber collisions were observed in SEQUELS and given the target class SEQUELS_COLLIDED. Observing these galaxies in SEQUELS creates large contiguous areas that have 100% spectroscopic completeness in the final BOSS data sample. A similar sample was described in Section A.2.

Variable targets selected from the PTF survey are targeted with the SEQUELS_PTF_VAR target class in three classes: hosts of supernovae detected in the PTF supernova program, RR Lyrae stars, and additional sources whose light curve built from PTF data show variations by 0.4 mag or more.

Emission-line galaxy candidates tend to have blue colors and thus are relatively bright in the u band. The South Galactic Cap U-band Sky Survey[154] (SCUSS) was carried out over the SEQUELS area using the 2.3 m Bok Telescope at Kitt Peak to obtain deeper data ($u \approx 23$ for 5 σ detections of point sources) than SDSS (X. Zhou et al. 2015, in preparation; H. Zou et al. 2015, in preparation). We used these data together with SDSS g, r, i photometry to select ELGs in the redshift range $0.4 < z < 1.6$ in a region of the sky of 25.7 deg^2 around $(\alpha, \delta) \sim (23°, 20°)$.

The brightest and bluest galaxy population (SEQUELS_ELG) is selected by

$$-0.5 < u - r < 0.7(g - i) + 0.1 \;\&\&\; 20 < u < 22.5$$

To fill the remaining fibers we also observed targets satisfying broader color cuts (SEQUELS_ELG_LOWP):

$$(20 < u < 22.7 \;\&\; -0.9 < u - r) \;\&(u - r < 0.7(g - i) + 0.2 \,||u - r < 0.7).$$

[154] http://batc.bao.ac.cn/Uband/

REFERENCES

Abazajian, K., Adelman-McCarthy, J. K., Agüeros, M. A., et al. 2003, AJ, 126, 2081
Abazajian, K., Adelman-McCarthy, J. K., Agüeros, M. A., et al. 2004, AJ, 128, 502
Abazajian, K., Adelman-McCarthy, J. K., Agüeros, M. A., et al. 2005, AJ, 129, 1755
Abazajian, K. N., Adelman-McCarthy, J. K., Agüeros, M. A., et al. 2009, ApJS, 182, 543
Adelman-McCarthy, J. K., Agüeros, M. A., Allam, S. S., et al. 2006, ApJS, 162, 38
Adelman-McCarthy, J. K., Agüeros, M. A., Allam, S. S., et al. 2007, ApJS, 172, 634
Adelman-McCarthy, J. K., Agüeros, M. A., Allam, S. S., et al. 2008, ApJS, 175, 297
Ahn, C. P., Alexandroff, R., Allende Prieto, C., et al. 2012, ApJS, 203, 21
Ahn, C. P., Alexandroff, R., Allende Prieto, C., et al. 2014, ApJS, 211, 17
Aihara, H., Allende Prieto, C., An, D., et al. 2011, ApJS, 193, 29
Anderson, L., Aubourg, É, Bailey, S., et al. 2014a, MNRAS, 441, 24
Anderson, L., Aubourg, É, Bailey, S., et al. 2014b, MNRAS, 441, 24
Anderson, L., Aubourg, É., Bailey, S., et al. 2014c, MNRAS, 439, 83
Annis, J., Soares-Santos, M., Strauss, M. A., et al. 2014, ApJ, 794, 120
Astropy Collaboration, Robitaille, T. P., Tollerud, E. J., et al. 2013, A&A, 558, A33
Aubourg, É., Bailey, S., Bautista, J. E., et al. 2014, PhRvD, submitted (arXiv:1411.1074)
Baglin, A., Auvergne, M., Barge, P., et al. 2002, in Proc. First Eddington Workshop on Stellar Structure and Habitable Planet Finding, ed. B. Battrick et al. (ESA SP-485; Noordwijk: ESA), 17
Bautista, J. E., Bailey, S., Font-Ribera, A., et al. 2014, JCAP, submitted (arXiv:1412.0658)
Becker, R. H., White, R. L., & Helfand, D. J. 1995, ApJ, 450, 559
Beutler, F., Saito, S., Brownstein, J. R., et al. 2014a, MNRAS, 444, 3501
Beutler, F., Saito, S., Seo, H.-J., et al. 2014b, MNRAS, 443, 1065
Bolton, A. S., Schlegel, D. J., Aubourg, É., et al. 2012, AJ, 144, 144
Bovy, J., Hennawi, J. F., Hogg, D. W., et al. 2011, ApJ, 729, 141
Bovy, J., Myers, A. D., Hennawi, J. F., et al. 2012, ApJ, 749, 41
Bovy, J., Nidever, D. L., Rix, H.-W., et al. 2014, ApJ, 790, 127
Budavári, T., & Szalay, A. S. 2008, ApJ, 679, 301
Bundy, K., Bershady, M. A., Law, D. R., et al. 2015, ApJ, 798, 7
Burke, C. J., Bryson, S. T., Mullally, F., et al. 2014, ApJS, 210, 19
Busca, N. G., Delubac, T., Rich, J., et al. 2013, A&A, 552, A96
Butler, R. P., Johnson, J. A., Marcy, G. W., et al. 2006, PASP, 118, 1685
Casagrande, L., Ramírez, I., Meléndez, J., Bessell, M., & Asplund, M. 2010, A&A, 512, A54
Chojnowski, S. D., Whelan, D. G., Wisniewski, J. P., et al. 2015, AJ, 149, 7
Chornock, R., Berger, E., Rest, A., et al. 2013, ApJ, 767, 162
Clerc, N., Sadibekova, T., Pierre, M., et al. 2012, MNRAS, 423, 3561

Collier Cameron, A., Wilson, D. M., West, R. G., et al. 2007, MNRAS, 380, 1230
Comparat, J., Richard, J., Kneib, J.-P., et al. 2015, A&A, 575, A40
Cottaar, M., Covey, K. R., Meyer, M. R., et al. 2014, ApJ, 794, 125
Coupon, J., Ilbert, O., Kilbinger, M., et al. 2009, A&A, 500, 981
Dawson, K. S., Schlegel, D. J., Ahn, C. P., et al. 2013, AJ, 145, 10
de Bruijne, J. H. J. 2012, Ap&SS, 341, 31
Delubac, T., Bautista, J. E., Busca, N. G., et al. 2015, A&A, 574, A59
Dhital, S., West, A. A., Stassun, K. G., & Bochanski, J. J. 2010, AJ, 139, 2566
Dhital, S., West, A. A., Stassun, K. G., et al. 2012, AJ, 143, 67
Dhital, S., West, A. A., Stassun, K. G., Schluns, K., & Massey, A. P. 2015, AJ, in press (arXiv:1504.0529)
Dressing, C. D., & Charbonneau, D. 2013, ApJ, 767, 95
Eisenstein, D. J., Annis, J., Gunn, J. E., et al. 2001, AJ, 122, 2267
Eisenstein, D. J., Weinberg, D. H., Agol, E., et al. 2011, AJ, 142, 72
Emerson, J. P., Sutherland, W. J., McPherson, A. M., et al. 2004, Msngr, 117, 27
Epstein, C. R., Elsworth, Y. P., Johnson, J. A., et al. 2014, ApJL, 785, L28
Erskine, D. J., & Ge, J. 2000, in ASP Conf. Ser. 195, Imaging the Universe in Three Dimensions, ed. W. van Breugel, & J. Bland-Hawthorn (San Francisco, CA: ASP), 501
Fan, X. 1999, AJ, 117, 2528
Filiz, Ak, N., Brandt, W. N., Hall, P. B., et al. 2012, ApJ, 757, 114
Filiz, Ak, N., Brandt, W. N., Hall, P. B., et al. 2013, ApJ, 777, 168
Finkbeiner, D. P., Padmanabhan, N., Schlegel, D. J., et al. 2004, AJ, 128, 2577
Finkbeiner, D. P., Schlafly, E., & Green, G. 2014, AAS, 223, 11614
Fleming, S. W., Ge, J., Barnes, R., et al. 2012, AJ, 144, 72
Font-Ribera, A., Kirkby, D., Busca, N., et al. 2014, JCAP, 5, 27
Foster, J. B., Cottaar, M., Covey, K. R., et al. 2015, ApJ, 799, 136
Frieman, J. A., Bassett, B., Becker, A., et al. 2008, AJ, 135, 338
Garn, T., Green, D. A., Riley, J. M., & Alexander, P. 2008, MNRAS, 383, 75
Gaulme, P., McKeever, J., Rawls, M. L., et al. 2013, ApJ, 767, 82
Ge, J. 2002, ApJL, 571, L165
Ge, J., Erskine, D. J., & Rushford, M. 2002, PASP, 114, 1016
Ge, J., Lee, B., de Lee, N., et al. 2009, Proc. SPIE, 7440, 0
Ge, J., van Eyken, J., Mahadevan, S., et al. 2006, ApJ, 648, 683
Georgakakis, A., & Nandra, K. 2011, MNRAS, 414, 992
Gibson, R. R., Brandt, W. N., & Schneider, D. P. 2008, ApJ, 685, 773
Gil-Marín, H., Noreña, J., Verde, L., et al. 2014a, MNRAS, in press (arXiv:1407.5668)
Gil-Marín, H., Verde, L., Noreña, J., et al. 2014b, MNRAS, in press (arXiv:1408.0027)
Gilmore, G., Randich, S., Asplund, M., et al. 2012, Msngr, 147, 25
Green, P. 2013, ApJ, 765, 12
Grether, D., & Lineweaver, C. H. 2006, ApJ, 640, 1051
Grier, C. J., Hall, P. B., Brandt, W. N., et al. 2015, ApJ, 806, 111
Gunn, J. E., Carr, M., Rockosi, C., et al. 1998, AJ, 116, 3040
Gunn, J. E., Siegmund, W. A., Mannery, E. J., et al. 2006, AJ, 131, 2332
Guo, H., Zehavi, I., & Zheng, Z. 2012, ApJ, 756, 127
Guo, H., Zheng, Z., Zehavi, I., et al. 2015, MNRAS, 446, 578
Hennawi, J. F., Myers, A. D., Shen, Y., et al. 2010, ApJ, 719, 1672
Hennawi, J. F., Strauss, M. A., Oguri, M., et al. 2006, AJ, 131, 1
Høg, E., Fabricius, C., Makarov, V. V., et al. 2000, A&A, 355, L27
Holtzman, J. A., Shetrone, M., Johnson, J. A., et al. 2015, AJ, submitted (arXiv:1501.04110)
Humphreys, E. M. L., Reid, M. J., Moran, J. M., Greenhill, L. J., & Argon, A. L. 2013, ApJ, 775, 13
Ilbert, O., Arnouts, S., McCracken, H. J., et al. 2006, A&A, 457, 841
Ivezić, Ž, Smith, J. A., Miknaitis, G., et al. 2007, AJ, 134, 973
Ju, W., Greene, J. E., Rafikov, R. R., Bickerton, S. J., & Badenes, C. 2013, ApJ, 777, 44
Kaiser, N., Aussel, H., Burke, B. E., et al. 2002, Proc. SPIE, 4836, 154
Kaiser, N., Burgett, W., Chambers, K., et al. 2010, Proc. SPIE, 7733, 0
Kasliwal, M. M. 2011, PhD thesis, California Institute of Technology
Kim, D.-W., Protopapas, P., Byun, Y.-I., et al. 2011, ApJ, 735, 68
Lang, D. 2014, AJ, 147, 108
Lang, D., Hogg, D. W., & Schlegel, D. J. 2014, arXiv:1410.7397
Law, N. M., Kulkarni, S. R., Dekany, R. G., et al. 2009, PASP, 121, 1395
Lee, B. L., Ge, J., Fleming, S. W., et al. 2011, ApJ, 728, 32
Lee, K.-G., Hennawi, J. F., Spergel, D. N., et al. 2015, ApJ, 799, 196
Lee, Y. S., Beers, T. C., Sivarani, T., et al. 2008, AJ, 136, 2022
Li, N., & Thakar, A. R. 2008, AIP Computing in Science & Engineering, 10, 18
Luo, B., Brandt, W. N., Eracleous, M., et al. 2013, MNRAS, 429, 1479
Ma, B., Ge, J., Barnes, R., et al. 2013, AJ, 145, 20
Mack, C. E., III, Ge, J., Deshpande, R., et al. 2013, AJ, 145, 139
Mészáros, S., Allende Prieto, C., Edvardsson, B., et al. 2012, AJ, 144, 120
Monet, D. G., Levine, S. E., Canzian, B., et al. 2003, AJ, 125, 984
Myers, A. D., Richards, G. T., Brunner, R. J., et al. 2008, ApJ, 678, 635
Neilsen, E. H., Jr. 2008, AIP Computing in Science & Engineering, 10, 13
Nidever, D. L., Bovy, J., Bird, J. C., et al. 2014, ApJ, 796, 38
Nidever, D. L., Holtzman, J. A., Allende Prieto, C., et al. 2015, AJ, submitted (arXiv:1501.03742)
Padmanabhan, N., Schlegel, D. J., Finkbeiner, D. P., et al. 2008, ApJ, 674, 1217
Paegert, M., Stassun, K. G., De Lee, N., et al. 2015, AJ, in press
Palanque-Delabrouille, N., Yeche, C., Myers, A. D., et al. 2011, A&A, 530, A122
Pancino, E., & Gaia-ESO Survey consortium 2012, arXiv:1206.6291
Pâris, I., Petitjean, P., Aubourg, et al. 2014, A&A, 563, A54
Prša, A., Batalha, N., Slawson, R. W., et al. 2011, AJ, 141, 83
Reid, B. A., Seo, H.-J., Leauthaud, A., Tinker, J. L., & White, M. 2014, MNRAS, 444, 476
Richards, G. T., Fan, X., Newberg, H. J., et al. 2002, AJ, 123, 2945
Richards, G. T., Myers, A. D., Gray, A. G., et al. 2009, ApJS, 180, 67
Riess, A. G., Macri, L., Casertano, S., et al. 2011, ApJ, 730, 119
Ross, N. P., Myers, A. D., Sheldon, E. S., et al. 2012, ApJS, 199, 3
Rykoff, E. S., Rozo, E., Busha, M. T., et al. 2014, ApJ, 785, 104
Sadibekova, T., Pierrre, M., Clerc, N., et al. 2014, A&A, 571, A87
Samushia, L., Reid, B. A., White, M., et al. 2014, MNRAS, 439, 3504
Sánchez, A. G., Montesano, F., Kazin, E. A., et al. 2014, MNRAS, 440, 2692
Schlafly, E. F., Finkbeiner, D. P., Jurić, M., et al. 2012, ApJ, 756, 158
Schlegel, D. J., Finkbeiner, D. P., & Davis, M. 1998, ApJ, 500, 525
Schneider, D. P., Richards, G. T., Hall, P. B., et al. 2010, AJ, 139, 2360
Shen, Y., Brandt, W. N., Dawson, K. S., et al. 2015a, ApJS, 216, 4
Shen, Y., Greene, J. E., Ho, L. C., et al. 2015b, ApJ, arXiv:1502.01034
Shetrone, M., Bizyaev, D., Lawler, J., et al. 2015, ApJS, submitted (arXiv:1502.04080)
Skrutskie, M. F., Cutri, R. M., Stiening, R., et al. 2006, AJ, 131, 1163
Slawson, R. W., Prša, A., Welsh, W. F., et al. 2011, AJ, 142, 160
Slosar, A., Iršič, V., Kirkby, D., et al. 2013, JCAP, 4, 26
Smee, S. A., Gunn, J. E., Uomoto, A., et al. 2013, AJ, 146, 32
Song, Y.-S., Sabiu, C. G., Okumura, T., Oh, M., & Linder, E. V. 2014, JCAP, 12, 5
Stassun, K. G., Mathieu, R. D., Cargile, P. A., et al. 2008, Natur, 453, 1079
Steinmetz, M., Zwitter, T., Siebert, A., et al. 2006, AJ, 132, 1645
Stoughton, C., Lupton, R. H., Bernardi, M., et al. 2002, AJ, 123, 485
Strateva, I. V., Brandt, W. N., Eracleous, M., Schneider, D. P., & Chartas, G. 2006, ApJ, 651, 749
Strauss, M. A., Weinberg, D. H., Lupton, R. H., et al. 2002, AJ, 124, 1810
Tasse, C., le Borgne, D., Röttgering, H., et al. 2008, A&A, 490, 879
Taylor, A. R., Bhatnagar, S., Condon, J., et al. 2014, arXiv:1405.0117
Thakar, A. R. 2008a, AIP Computing in Science & Engineering, 10, 65
Thakar, A. R. 2008b, AIP Computing in Science & Engineering, 10, 9
Thakar, A. R., Szalay, A., Fekete, G., & Gray, J. 2008, AIP Computing in Science & Engineering, 10, 30
Tojeiro, R., Ross, A. J., Burden, A., et al. 2014, MNRAS, 440, 2222
van Eyken, J. C., Ge, J., & Mahadevan, S. 2010, ApJS, 189, 156
van Haarlem, M. P., Wise, M. W., Gunst, A. W., et al. 2013, A&A, 556, A2
Véron-Cetty, M.-P., & Véron, P. 2010, A&A, 518, A10
Voges, W., Aschenbach, B., Boller, T., et al. 1999, A&A, 349, 389
Voges, W., Aschenbach, B., Boller, T., et al. 2000a, IAU Circ., 7432, 1
Voges, W., Aschenbach, B., Boller, T., et al. 2000b, yCat, 9029, 0
Wisniewski, J. P., Ge, J., Crepp, J. R., et al. 2012, AJ, 143, 107
Wright, E. L., Eisenhardt, P. R. M., Mainzer, A. K., et al. 2010, AJ, 140, 1868
Wright, J. T., Fischer, D. A., Ford, E. B., et al. 2009, ApJL, 699, L97
Yanny, B., Rockosi, C., Newberg, H. J., et al. 2009, AJ, 137, 4377
Yèche, C., Petitjean, P., Rich, J., et al. 2010, A&A, 523, A14
York, D. G., Adelman, J., Anderson, J. E., Jr., et al. 2000, AJ, 120, 1579
Zamora, O., Garcia-Hernandez, D. A., Allende Prieto, C., et al. 2015, AJ, 149, 181
Zasowski, G., Johnson, J. A., Frinchaboy, P. M., et al. 2013, AJ, 146, 81
Zasowski, G., Ménard, B., Bizyaev, D., et al. 2015, ApJ, 798, 35
Zhu, G., Zaw, I., Blanton, M. R., & Greenhill, L. J. 2011, ApJ, 742, 73